ผลกระทบของค่ารีพิทชั่นไทม์ (Repetition time: TR) ต่อการวัดค่า
ทีทู (T_2 relaxation time) ของกล้ามเนื้อ เพื่อการตรวจสอบการทำงานของกล้ามเนื้อ
ในเครื่องถ่ายภาพสนามแม่เหล็กกำทอน 1.5 เทสลา

นายปฐมพงศ์ พลหาญ

วิทยานิพนธ์นี้เป็นส่วนหนึ่งของการศึกษาตามหลักสูตรปริญญาวิทยาศาสตรมหาบัณฑิต
สาขาวิชาฉายาเวชศาสตร์ ภาควิชารังสีวิทยา
คณะแพทยศาสตร์ จุฬาลงกรณ์มหาวิทยาลัย
ปีการศึกษา 2559

The Effect of Repetition Time during The Measurement of Muscle T_2 for Investigating Muscle Activity at 1.5 Tesla MRI

Mr. Patompong Polharn

A Thesis Submitted in Partial Fulfillment of the Requirements
for the Degree of Master of Science Program in Medical Imaging
Department of Radiology
Faculty of Medicine
Chulalongkorn University
Academic Year 2016

Thesis Title	The Effect of Repetition Time during The Measurement of Muscle T_2 for Investigating Muscle Activity at 1.5 Tesla MRI
By	Mr. Patompong Polharn
Field of Study	Medical Imaging
Thesis Advisor	Associate Professor Anchali Krisanachinda, Ph.D.
Thesis Co-Advisor	Professor Noriyuki Tawara, Ph.D.

Accepted by the Faculty of Medicine, Chulalongkorn University in Partial Fulfillment of the Requirements for the Master's Degree

.....Dean of the Faculty of Medicine
(Professor Suttipong Wacharasindhu, M.D.)

THESIS COMMITTEE

.....Chairman
(Kitiwat Khamwan, Ph.D.)

.....Thesis Advisor
(Associate Professor Anchali Krisanachinda, Ph.D.)

.....Thesis Co-Advisor
(Professor Noriyuki Tawara, Ph.D.)

.....External Examiner
(Professor Franco Milano, Ph.D.)

.....External Examiner
(Associate Professor Kosuke Matsubara, Ph.D.)

ปฐมพงศ์ พลหาญ : ผลกระทบของค่ารีพิทิชั่นไทม์ (Repetition time: TR) ต่อการวัดค่าทีทู (T_2 relaxation time) ของกล้ามเนื้อ เพื่อการตรวจสอบการทำงานของกล้ามเนื้อ ในเครื่องถ่ายภาพสนามแม่เหล็กกำทอน 1.5 เทสลา (The Effect of Repetition Time during The Measurement of Muscle T_2 for Investigating Muscle Activity at 1.5 Tesla MRI) อ.ที่ปรึกษาวิทยานิพนธ์หลัก: รศ. ดร.อัญชลี กฤษณจินดา, อ.ที่ปรึกษาวิทยานิพนธ์ร่วม: ศ. ดร.โนริยูกิ ทาวาร่า, 76 หน้า.

การประเมินสมรรถภาพของกล้ามเนื้อโดยการสร้างภาพแผนที่ทีทู (T_2 mapping) เป็นสิ่งสำคัญในเวชศาสตร์การกีฬาและเวชศาสตร์ฟื้นฟู ค่ารีพิทิชั่นไทม์ (Repetition time: TR) เป็นหนึ่งในตัวแปรที่มีความสำคัญต่อการคำนวณค่าทีทู (T_2) และมีผลต่อความถูกต้องในการวัดค่าทีทู (T_2) จากการศึกษาก่อนหน้านี้ส่วนใหญ่จะเลือกใช้ลำดับพัลส์สปินเอคโค่ (Spin echo: SE) หรือมัลติเปิ้ลสปินเอคโค่ (Multiple spin echo: MSE) ในการคำนวณค่าทีทู (T_2) มีรายงานจำนวนน้อยที่ศึกษาเกี่ยวกับการเปรียบเทียบค่าตัวแปรที่มีผลต่อการวัดค่าทีทู (T_2) โดยใช้ลำดับพัลส์สปินเอคโค่เอคโค่พลาน่า (Spin echo echo-planar imaging: SE-EPI) ดังนั้นวัตถุประสงค์ของการศึกษานี้คือ 1) ศึกษาผลกระทบของค่ารีพิทิชั่นไทม์ (TR) เพื่อลดเวลาในการสแกนต่อการวัดค่าทีทู (T_2) ของกล้ามเนื้อโดยการเปรียบเทียบลำดับพัลส์ในเครื่องถ่ายภาพสนามแม่เหล็กกำทอน 1.5 เทสลา 2) ประเมินความเป็นไปได้ในการใช้เทคนิคการลดเวลาการสแกนในการวัดค่าทีทู (T_2) เพื่อตรวจสอบการทำงานของกล้ามเนื้อที่เกิดจากการออกกำลังกาย ทำการศึกษาโดยการสแกนหุ่นจำลอง (PVA-gel phantom) และขาขวาของอาสาสมัครชายที่มีสุขภาพดีจำนวน 8 คน โดยใช้เครื่องถ่ายภาพสนามแม่เหล็กกำทอน 1.5 เทสลาและใช้ลำดับพัลส์ MSE และ SE-EPI ร่วมกับค่ารีพิทิชั่นไทม์ (TR) 1,000, 2,000, ..., 4,000 มิลลิวินาที เอคโค่ไทม์ (TE) 15, 30, ..., 390 มิลลิวินาที ในการประเมินความเป็นไปได้ของลำดับพัลส์ SE-EPI เพื่อตรวจสอบการทำงานของกล้ามเนื้อ อาสาสมัครทำการออกกำลังกายโดยการงอข้อเท้าจำนวน 200 ครั้ง ทำการสแกนขาขวาของอาสาสมัครทั้งก่อนและหลังออกกำลังกาย คำนวณค่าทีทู (T_2) โดยใช้วิธี mono-exponential linear least-squares ของค่าเอคโค่ไทม์ (TE) ที่ 30, 45, 60, 75 มิลลิวินาที

ผลการศึกษาในหุ่นจำลองและอาสาสมัครให้ผลการทดลองไปในทางเดียวกัน สำหรับ MSE, relaxation curve ของค่ารีพิทิชั่นไทม์ (TR) ที่มากกว่า 2,000 มิลลิวินาที แสดงให้เห็นถึง relaxation curve ที่มีความใกล้เคียงกัน สำหรับ SE-EPI, relaxation curve ของทุกค่ารีพิทิชั่นไทม์ (TR) แทบจะซ้อนทับกัน เมื่อนำ relaxation curve ของทั้งสองลำดับพัลส์มาเปรียบเทียบกัน พบว่า relaxation curve ของ SE-EPI ในทุกค่ารีพิทิชั่นไทม์ (TR) ให้สัญญาณที่ต่ำกว่า MSE แต่อย่างไรก็ตามเมื่อนำค่าทีทู (T_2) ของทั้งสองลำดับพัลส์และทุกค่ารีพิทิชั่นไทม์ (TR) มาเปรียบเทียบกัน พบว่าไม่มีความแตกต่างอย่างมีนัยสำคัญทางสถิติ สำหรับผลการศึกษาการออกกำลังกาย พบว่าค่าทีทู (T_2) ของกล้ามเนื้อ gastrocnemius หลังออกกำลังกายมีค่ามากกว่าก่อนออกกำลังกายอย่างมีนัยสำคัญทางสถิติ สรุปผลการทดลอง ภาพเอ็มอาร์ไอที่ได้จากค่ารีพิทิชั่นไทม์ (TR) ที่สั้นลง (TR 1,000 มิลลิวินาที) ภายใต้คุณสมบัติที่เหมาะสมสามารถนำมาใช้เพื่อคำนวณค่าทีทู (T_2) ของกล้ามเนื้อเพื่อลดเวลาในการสแกนได้อย่างมีประสิทธิภาพ ลำดับพัลส์ SE-EPI สามารถนำมาใช้ในการคำนวณค่าทีทู (T_2) เพื่อตรวจสอบการทำงานของกล้ามเนื้อหลังออกกำลังกายได้และสามารถลดเวลาในการสแกนได้อย่างมีประสิทธิภาพถึง 1/17 เท่า เทียบกับงานวิจัยก่อนหน้านี้

ภาควิชา รังสีวิทยา	ลายมือชื่อนิสิต .....
สาขาวิชา ฉายาเวชศาสตร์	ลายมือชื่อ อ.ที่ปรึกษาหลัก .....
ปีการศึกษา 2559	ลายมือชื่อ อ.ที่ปรึกษาร่วม .....

5874042730 : MAJOR MEDICAL IMAGING
KEYWORDS: TRANSVERSE RELAXATION TIME (T2) / REPETITION TIME (TR) / MULTIPLE SPIN ECHO (MSE) / SPIN ECHO-ECHO PLANAR IMAGING (SE-EPI) / MUSCLE FUNCTIONAL MRI (MFMRI)

PATOMPONG POLHARN: The Effect of Repetition Time during The Measurement of Muscle T_2 for Investigating Muscle Activity at 1.5 Tesla MRI. ADVISOR: ASSOC. PROF. ANCHALI KRISANACHINDA, Ph.D., CO-ADVISOR: PROF. NORIYUKI TAWARA, Ph.D., 76 pp.

The evaluation of muscle function by T_2 mapping is important in sports medicine and rehabilitation. Repetition time (TR) is one of the most important parameters for calculating T_2 and affects the accurate T_2 measurements. The previous study used SE or MSE to calculate T_2 and there were few reports about the extensive comparative evaluation of the imaging parameters using SE-EPI. Thus, the goals of this study were 1) to evaluate the effect of TR in decreasing scan time for muscle T_2 measurement in the pulse sequences at 1.5 Tesla MRI and 2) to investigate the feasibility of shortening scan time of T_2 measurement to detect the muscle activity that induced by exercise. A PVA-gel phantom and right lower legs of eight healthy male subjects were scanned using a 1.5 tesla MR scanner. MSE and SE-EPI were performed with TR 1,000, 2,000, ..., 4,000 ms, TE 15, 30, ..., 390 ms. To evaluate the feasibility of SE-EPI to detect muscle activity. Subject performed ankle plantar flexion of the right leg 200 times and MR images were acquired at rest and after exercise. T_2 was calculated by mono-exponential linear least-squares of TE 30, 45, 60, 75 ms.

Phantom and in vivo: comparison studies showed the result in the same way. For MSE, the relaxation curve of TR 2,000 ms or more is likely to be the same MR signal. For SE-EPI, all relaxation curve showed approximately the same MR signal and all SE-EPI's MR signal were lower than the signals of MSE. However, all of T_2 have no significant difference between TR and sequences. Regarding in vivo: exercise study, T_2 of gastrocnemius muscle at after exercise was significantly higher than T_2 at rest. In conclusion, MR images with a short TR (TR 1,000 ms) under suitable condition are possible to calculate muscle T_2 to reduce the scan time dramatically. Calculating T_2 using SE-EPI, can be applied to detect the muscle activity that induced by exercise with the shortening acquisition time of approximately 1/17 of the previous methods.

Department:	Radiology	Student's Signature	.....
Field of Study:	Medical Imaging	Advisor's Signature	.....
Academic Year:	2016	Co-Advisor's Signature	.....

ACKNOWLEDGEMENTS

I would like to express gratitude and deepest appreciation to Associate Professor Anchali Krisanachinda, Ph.D., Department of Radiology, Faculty of Medicine, Chulalongkorn University, my advisor, for her guidance, helpful suggestion, supervision, constructive comments and polishing of the thesis writing to improve the readability and English expression.

I would like to extremely grateful Professor Noriyuki Tawara, Ph.D., Department of Radiological Sciences, Faculty of Health Sciences, Japan Health Care College, Japan, my co-advisor for his advice and comments that opened up a new perspective on the MRI research.

I would like to extremely thank Miss Kanokvalee Ponkanist, M.Sc., Medical Physics staff at Department of Radiology, King Chulalongkorn Memorial Hospital, for good advice, comments and contribute in part of the data collection on the research.

I would like to extremely thank Mr. Kitiwat Khamwan, Ph.D., Department of Radiology, Faculty of Medicine, Chulalongkorn University, for his advice and comments in the research.

I am extremely grateful Associate Professor Sivalee Suriyapee, M.Eng., Department of Radiology, Faculty of Medicine, Chulalongkorn University, my teacher for her invaluable advice, constructive comments.

I would like to extremely thank Mr. Taweap Sanghangthum, Ph.D., Division of Radiation Oncology, Department of Radiology, King Chulalongkorn Memorial Hospital, my teacher for his invaluable advice, constructive comments.

I would like to deeply thank Associate Professor Kosuke Matsubara, Ph.D. from Kanazawa University, Japan, and Professor Franco Milano, Ph.D. from University of Florence Italy, External examiner of this thesis defense for his helpful recommendations, constructive comments and teaching in Medical Imaging.

I would like to thank Mrs. Weeranuch Kitsukjit for her suggestion for the improvement.

Finally, I am extremely grateful for all teachers, lectures and staffs at Master of Science in Medical Imaging, Faculty of Medicine, Chulalongkorn University for their help, and unlimited teaching during the course in Medical Imaging

CONTENTS

Page

THAI ABSTRACT iv

ENGLISH ABSTRACT v

ACKNOWLEDGEMENTS vi

CONTENTS vii

LIST OF TABLES xi

LIST OF FIGURES xiii

LIST OF ABBREVIATIONS xviii

CHAPTER 1 1

INTRODUCTION 1

1.1 Background and rationale 1

1.2 Research objectives 2

CHAPTER 2 3

REVIEW OF RELATED LITERATURE 3

2.1 Theory 3

2.1.1 Behavior in an external magnetic field 4

2.1.2 Measuring the net magnetization 6

2.1.3 Relaxation process 7

2.1.4 Spatial localization 10

2.1.5 The data matrix (k-space) 12

2.1.6 Pulse sequences 13

2.1.7 MR equipment 16

2.2 The introduction of muscle functional MRI 19

Page

2.2.1 Mechanism of mfMRI 19
2.2.2 Measurement protocols 20
2.3 Review of related literature 22
CHAPTER 3 26
RESEARCH METHODOLOGY 26
3.1 Research design 26
3.2 Research design models 26
3.2.1 Phantom study 26
3.2.2 In vivo study 27
3.2.2.1 Comparison study 27
3.2.2.2 Exercise study 27
3.3 Conceptual framework 28
3.4 Research questions 28
3.4.1 Primary research question 28
3.4.2 Secondary research question 28
3.5 The sample 28
3.5.1 Target population 28
3.5.2 Sample population 28
3.5.3 Eligible criteria 29
3.5.3.1 Inclusion criteria 29
3.5.3.2 Exclusion criteria 29
3.5.4 Sample size determination 29
3.6 Materials 30

Page

3.6.1 MRI 1.5 Tesla whole body scanner, Siemens, MAGNETOM Aera 30
3.6.2 The 20-channel head/neck phase array coil 30
3.6.3 ACR MRI accreditation phantom 31
3.6.4 CP extremity coil 31
3.6.5 PVA-gel phantom 32
3.6.6 Siemens Syngo workstation software 32
3.7 Methods 33
3.7.1 Quality control of MRI scanner 33
3.7.2 Phantom study 33
3.7.2 In vivo study 34
3.7.2.1 Comparison study 34
3.7.2.2 Exercise study 34
3.8 Data analysis 35
3.8.1 Data analysis of phantom and in vivo: comparison studies 35
3.8.2 Data analysis of in vivo: exercise study 36
3.9 Statistical analysis 36
3.9.1 Statistical analysis of phantom and in vivo: comparison studies 36
3.9.2 Statistical analysis of in vivo: exercise study 36
3.10 Outcome measurement 36
3.11 Expected benefit 37
3.12 Ethical consideration 37
3.13 Limitation 38
CHAPTER 4 39

Page

RESULTS 39
4.1 Quality control of MRI scanner 39
4.2 Phantom study data 40
4.3 In vivo study data 43
4.3.1 Comparison study data 43
4.3.2 Exercise study data 46
CHAPTER 5 49
DISCUSSION AND CONCLUSIONS 49
5.1 Discussion 49
5.1.1 Phantom study 49
5.1.2 In vivo: comparison study 50
5.1.3 In vivo: exercise study 51
5.2 Conclusions 51
REFERENCES 52
APPENDICES 55
Appendix A: Case record form 56
Appendix B: Quality control of MRI scanner 62
B.1. Geometric accuracy 64
B.2. High contrast spatial resolution 65
B.3. Slice thickness accuracy 66
B.4. Slice position accuracy 68
B.5. Image intensity uniformity 70
B.6. Percent signal ghosting 72

Page

B.7. Low contrast object detectability 73

Appendix C: T_2 calculation method 75

VITA 76

LIST OF TABLES

Table **Page**

3.1 Pulse sequences parameters of phantom and in vivo: comparison studies 33

3.2 Pulse sequences parameters of in vivo: exercise study 35

4.1 Report of MRI 1.5 Tesla performance test 39

4.2 T_2 of phantom study using MSE and SE-EPI by variation of TR 42

4.3 T_2 of phantom study using MSE and SE-EPI versus the percent difference values in each TR and sequences 42

4.4 T_2 of in vivo: comparison study from 8 healthy male volunteers using MSE and SE-EPI by four condition of TR 45

4.5 T_2 of in vivo: comparison study using MSE and SE-EPI versus the percent difference values in each TR and sequences 46

4.6 T_2 of in vivo: exercise study from 8 healthy male volunteers at rest and after exercise of tibialis anterior muscle [TA] and gastrocnemius muscle [GA] 47

4.7 The muscle T_2 at rest and after exercise of tibialis anterior muscle [TA] and gastrocnemius muscle [GA]. 47

A.1 Means signal intensities (Mean ± SD) in each TE of Phantom study 56

A.2 T_2 of phantom study using MSE and SE-EPI by variation of TR 57

A.3 T_2 of phantom study using MSE and SE-EPI versus the percent difference in each TR and sequences 57

A.4 Subject data of In vivo study 58

A.5 Means signal intensities in each TE of In vivo: Comparison study 59

A.6 T_2 of in vivo: comparison study using MSE and SE-EPI by variation of TR 60

Table **Page**

A.7 T_2 of in vivo: comparison study using MSE and SE-EPI versus the percent difference values in each TR and sequences..... 60

A.8 T_2 of in vivo: exercise study at rest and after exercise of tibialis anterior muscle [TA] and gastrocnemius muscle [GA]..... 61

A.9 T_2 at rest and after exercise of tibialis anterior muscle [TA] and gastrocnemius muscle [GA]..... 61

B.1 ACR Pulse sequence acquisition parameters..... 63

B.2 Geometric accuracy test result..... 64

B.3 High contrast spatial resolution result..... 65

B.4 Slice thickness accuracy test result..... 67

B.5 Slice position accuracy test result..... 69

B.6 Image intensity uniformity test result..... 71

B.7 Pixel value and Percent signal ghosting test result..... 72

B.8 Low contrast detectability test result..... 74

LIST OF FIGURES

Figure **Page**

2.1 A rotating nucleus with a positive charge produces a magnetic field which acts like a bar magnet (dipole). 3

2.2 A collection of protons in the absence of an externally applied magnetic field. The magnetic moments have random orientations (a). An external magnetic field B_0 is applied which causes the nuclei to align themselves in one of two orientations with respect to B_0 (denoted parallel and anti-parallel) (b). 4

2.3 Zeeman diagram. In the absence of a magnetic field (left side). In the presence of a magnetic field (right side), the spin up orientation is lower energy and it contains more protons than the higher energy, spin down. The difference in energy ΔE between the two levels is proportional to B_0. 5

2.4 Average of many protons produces the net magnetization M_0. 6

2.5 Energy absorption, the RF pulse at the resonant frequency can be treated as an additional magnetic field B_1 oriented perpendicular to B_0. When energy is applied at the appropriate frequency, the protons absorb it and M_0 rotates into the transverse plane. The direction of rotation is perpendicular to both B_0 and B_1. 7

2.6 After a RF pulse, M_0 lies in the transverse plane and rotates about the z-axis (a). The component of M_0 in the x-y plane decays over time. An alternating current is induced in the receiver coil (b). 7

2.7 The recovery of longitudinal magnetization (M_z) and its relation with the value of T_1. 8

2.8 The decay of transverse magnetization (M_{xy}) and its relation with the value of T_2. 9

Figure **Page**

2.9 A comparison of T_2 decay and the more rapid T_2* decay arising from magnet inhomogeneity. 9

2.10 Slice selection process. In the presence of a gradient (G_{SS}), the total magnetic field that a proton experiences and its resulting resonant frequency depend on its position. Tissue located at position z_i will absorb RF energy with a unique resonant frequency. The slice thickness Δz is determined by the amplitude of G_{SS} and by the bandwidth of transmitted frequencies. 10

2.11 Readout process. Following excitation, each proton within the excited volume (slice) precesses at the same frequency. During detection of the echo, a gradient (G_{RO}) is applied, causing a variation in the frequencies for the protons generating the echo signal. The frequency of precession ω_i for each proton depends upon its position x_i. 11

2.12 Concept of phase encoding. Prior to application of G_{PE}, all protons precess at the same frequency. When G_{PE} is applied, a proton increases or decreases its precessional frequency, depending on its position, y_i. A proton located at $y_i = 0$ (y_2) experiences no effect from G_{PE} ($\Phi_2 = 0$). A proton located at y_3 and y_1 increase and decrease its frequencies while G_{PE} is applied. Once G_{PE} is turned off, the proton precesses at its original frequency, but is ahead of the reference frequency (dashed curve); that is, a phase shift Φ_3 and Φ_1 has been induced. 11

2.13 The data matrix showing the central positioning of the signal acquired with the phase encoding gradient set to zero (a). The data matrix with further signals from different phase encoding steps included; each is shown in a different shade of gray. When all the data for an image have been acquired, there will be a signal in the data matrix for every phase encoding step. The value saved at each point in the data matrix represents the amplitude and phase of the signal at that location (b). 12

Figure **Page**

2.14 The components in a typical MR system..... 16

2.15 Three sets of wires. Each set can create a magnetic field in a specific direction: Z, X or Y. When a current is fed into the Z gradient, then a magnetic field is generated in the Z direction. The same goes for the other gradients..... 17

2.16 T_2 weighted image at rest (A) and following exercise (B) There is an increased signal intensity (brighter) for the m. multifidus (MF) and the m. erector spinae (ES). Although the changes in signal intensity are subtly visible, they are quantifiable using the calculation of T_2. 20

2.17 Percentage increase in signal intensity (SI) of flexor digitorum profundus (FDP) immediately after intense handgrip is shown for different pulse sequences**.**..... 22

2.18 Representative T_2 weighted images (A, B) and T_2 mapping images (C, D) of the right thigh before and after knee extension exercise. Specific exercise can be distinguished active and inactive muscle in muscle T_2 mapping images..... 24

2.19 Fusion images [fast-mfMRI]) produced from multiple spin-echo (MSE) (a) and spin-echo echo-planar imaging (SE-EPI) images (b). The bright areas on both images agree with each other (arrows). Areas of deep red color indicated where muscle activation greatest..... 25

3.1 Overview of research design model..... 26

3.2 Research design model of phantom study. 26

3.3 Research design model of in vivo: comparison study..... 27

3.4 Research design model of in vivo: exercise study. 27

3.5 Conceptual framework..... 28

3.6 MRI 1.5 Tesla (MAGNETOM Aera; Siemens AG, Erlangen, Germany). 30

Figure **Page**

3.7 The 20-channel head/neck phase array coil. 30

3.8 ACR MRI accreditation phantom. 31

3.9 CP extremity coil. 31

3.10 PVA-gel phantom (NIKKO FINES INDUSTRIES Co.,Ltd, Tokyo, Japan). 32

3.11 Siemens Syngo workstation software. 32

3.12 ROIs were placed on PVA-gel image (a) and axial MR image of right leg at tibialis anterior muscle [TA] (b). 35

3.13 ROIs were placed on muscle image at tibialis anterior muscle (a) and gastrocnemius muscle images (b). 36

4.1 T_2 relaxation curve of PVA-gel phantom using MSE. 40

4.2 T_2 relaxation curve of PVA-gel phantom using SE-EPI. 41

4.3 T_2 relaxation curve of PVA-gel phantom between MSE and SE-EPI. 41

4.4 T_2 relaxation curve of in vivo: comparison study using MSE. 43

4.5 T_2 relaxation curve of in vivo: comparison study using SE-EPI. 44

4.6 T_2 relaxation curve of in vivo: comparison study between MSE and SE-EPI. 44

4.7 Representative MR images of the right lower leg of SE-EPI at rest (a) and after exercise (b) and TrueFISP image at rest (c). The arrows indicate the areas of activated muscle. 46

B.1 The end-to-end length and diameter measurements illustrated. 64

B.2 Magnified portion of slice 1 displayed appropriately for visually assessing high contrast resolution. 65

B.3 ROIs placed for measuring average signal in the ramps. 66

B.4 Magnified region of slice 1 showing slice thickness signal ramps. 67

Figure **Page**

B.5 Images of slice 1 (a) and slice 11 (b) with the pairs of vertical bars from the 45° crossed wedges indicated. 68

B.6 Images of slice 1 illustrating measurement of slice position error. The arrows indicate the bar length difference measurement that is to be made. 69

B.7 ROI placement for low signal-value (right), ROI placement for High signal-value (left). 70

B.8 ROIs placement for percent-signal ghosting measurements..... 72

B.9 Image of slice 11 showing the circle of low contrast objects for the low-contrast object detectability test. 73

LIST OF ABBREVIATIONS

ABBREVIATION	TERMS
AAPM	American Association of Physicists in Medicine
ACR	American College of Radiologists
B_0	Magnetic field strength
B_1	Radio-frequency field strength
EPI	Echo planar imaging
FID	Free induction decay
FOV	Field of view
FSE	Fast spin echo
GA	Gastrocnemius
G_{PE}	Phase encoding gradient
GRE	Gradient echo
G_{RO}	Read-out gradient
G_{SS}	Slice selection gradient
IR	Inversion recovery
mfMRI	Muscle functional MRI
MRI	Magnetic resonance imaging
ms	millisecond
MSE	Multiple spin echo
NSA	Number of signal average
PVA	Polyvinyl alcohol
Px	Pixel
QC	Quality control
RF	Radiofrequency
ROI	Region of interest
SE	Spin echo
SE-EPI	Spin echo-echo planar imaging

ABBREVIATION	TERMS
T	Tesla
T_1	Longitudinal relaxation
T_2	Transverse relaxation
T_2*	T2 star
TA	Tibialis anterior
TE	Echo time
TR	Repetition time
TSE	Turbo spin echo
TrueFISP	True fast imaging with steady state precession

CHAPTER 1

INTRODUCTION

1.1 Background and rationale

Magnetic resonance imaging (MRI) has become the standard imaging modality to investigate anatomical information and function of muscles due to its ability to provide excellent soft tissue contrast, high spatial resolution and techniques to quantify function, composition, microstructure of muscles or group of muscles. In exercised physiology and/or sports medicine, MRI can be used to measure the changes in quantitative data of muscle activity that induced by specific exercise. In detail, signal intensities changes are measured in order to calculate transverse relaxation time (T_2) of muscle tissue to indicate exercise-induced muscle activity. This method is called muscle functional MRI (mfMRI) [1-4].

The mfMRI is noninvasive technique to measure the changes in transverse relaxation time (T_2) of muscle tissue after specific exercise. The technique generates the muscle T_2 mapping images that represent the variation in T_2 within the activated muscle. The difference in T_2 between rest and stress muscle after specific exercise make it possible to isolate the activated muscles or group of muscles. The mfMRI has proven to be a useful tool to confirm the extent of activated muscle after specific exercise. However, the physiological mechanism of increasing of T_2 during and after exercise is still not fully understood [1, 2]. Furthermore, although various items are involved in the acquisition condition of muscle T_2, the influence of those items remains unknown. Therefore, multiple factors are probably involved. Such as repetition time (TR), echo time (TE), the number of measurement point and the choice of RF coil, etc.

Repetition time (TR) is one of the most important parameters for calculating T_2 and extremely related with the scan time. Reduction of TR will effect on decreasing the scan time for acquiring the data. On the other hand, though short TR adversely affects to calculate T_2 as a traditional rule for the condition, it still remains an open research problem.

In pulse sequence, almost previous study about muscle functional MRI (mfMRI) used spin echo (SE) or multiple spin echo (MSE) sequences to calculate T_2 that usually require several minutes to acquire image data. In order to calculate T_2 by spin echo-echo planar imaging (SE-EPI) which is innovative technique and use to reduce acquisition time, there are few reports about the extensive comparative evaluation of the imaging parameters of SE-EPI sequence. Therefore, even from the viewpoint of selecting pulse sequence, the optimization of image conditions for T_2 measurement still remains controversial. So in this study we would like to investigate effect of TR on T_2 relaxation time of muscle tissue and study the feasibility of SE-EPI to detect the muscle activity that induced by exercise.

1.2 Research objectives

1.2.1 To evaluate the effect of the repetition time (TR) on decreasing scan time for muscle T_2 measurement comparing multiple spin echo (MSE) to spin echo-echo planar imaging (SE-EPI) at 1.5 Tesla MRI.

1.2.2 To investigate the feasibility of spin echo-echo planar imaging (SE-EPI) for muscle T_2 measurement to detect the muscle activity that induced by specific exercise.

CHAPTER 2

REVIEW OF RELATED LITERATURE

2.1 Theory

Magnetic resonance (MR) is based upon the interaction between an applied magnetic field and a nucleus that possesses spin. Nuclear spin or nuclear spin angular momentum is one of several intrinsic properties of an atom and its value depends on the precise atomic composition.

Atoms consist of three fundamental particles: protons, neutrons and electrons. The characteristic chemical reactions of elements depend upon the particular number of each of these particles. The properties most commonly used to categorize elements are the atomic number and the atomic weight. A third property of the nucleus is spin or intrinsic spin angular momentum. The nucleus can be considered to be constantly rotating about an axis at a constant rate. This self-rotation axis is perpendicular to the direction of rotation (Figure 2.1).

The ^{1}H nucleus, consisting of a single proton, is a natural choice for probing the body using MR techniques for several reasons. It has a spin of 1/2 and is the most abundant isotope for hydrogen. Its response to an applied magnetic field is one of the largest found in nature. Finally, the human body is composed of tissues that contain primarily water and fat, both of which contain hydrogen [5].

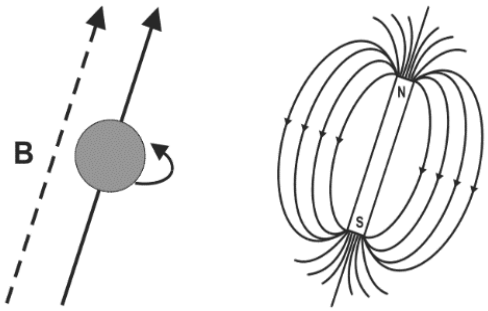

Figure 2.1 A rotating nucleus with a positive charge produces a magnetic field which acts like a bar magnet (dipole) [5].

2.1.1 Behavior in an external magnetic field

Consider an arbitrary volume of tissue containing hydrogen atoms (protons). The spin vectors for the entire collection of protons within the tissue are randomly oriented in all directions. The vector sum of these spin vectors is zero; that is, no net magnetization (Figure 2a). If the tissue is placed inside a magnetic field B_0, the individual protons begin to rotate perpendicular to the magnetic field. The protons are tilted slightly away from the axis of the magnetic field, but the axis of rotation is parallel to B_0 (Figure 2b). The rate or frequency of precession is proportional to the strength of the magnetic field and is expressed by the Larmor equation [5]:

$$\omega_0 = \frac{\gamma B_0}{2\pi} \tag{2.1}$$

where ω_0 is the Larmor frequency in megahertz (MHz), B_0 is the magnetic field strength in Tesla (T), and γ is a constant for each nucleus in MHz/T, known as the gyromagnetic ratio. The factor of 2π in is necessary to convert from angular to cyclical frequency.

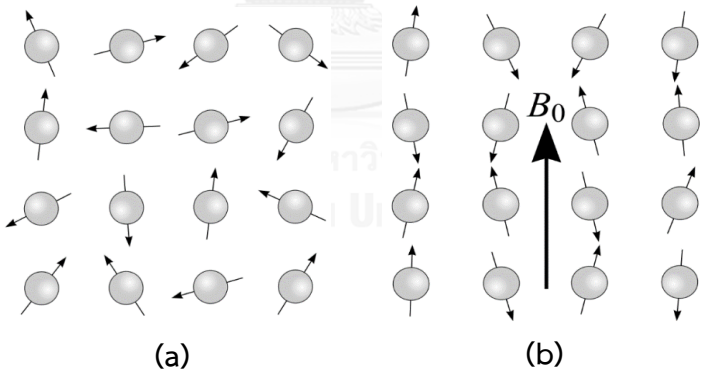

Figure 2.2 (a) A collection of protons in the absence of an externally applied magnetic field. The magnetic moments have random orientations. (b) An external magnetic field B_0 is applied which causes the nuclei to align themselves in one of two orientations with respect to B_0 (denoted parallel and anti-parallel) [6].

If a vector addition is performed for the spin vectors inside the magnetic field. In the direction parallel to the magnetic field, there is an orientation to the precessional axis of the proton that is constant with time or coupling between the proton and B_0. This is known as the Zeeman interaction. This coupling causes a difference in energy between protons aligned parallel and antiparallel to B_0. This energy difference ΔE is proportional to B_0 (Figure 2.3).

The result of the Zeeman interaction is that spins in the two orientations, parallel (spin up) and antiparallel (spin down), have different energies. The orientation that is parallel to B_0 is of lower energy than the antiparallel orientation. For a collection of protons, more will be oriented parallel to B_0 than antiparallel; that is, there is an induced polarization of the spin orientation by the magnetic field. The exact number of protons in each energy level is governed by a distribution known as the Boltzmann distribution:

$$\frac{N_{upper}}{N_{lower}} = e^{-\Delta E/kT} \tag{2.2}$$

where N_{upper} and N_{lower} are the number of protons in the upper and lower energy levels, respectively, and k is Boltzmann's constant, 1.381×10^{-23} J/K.

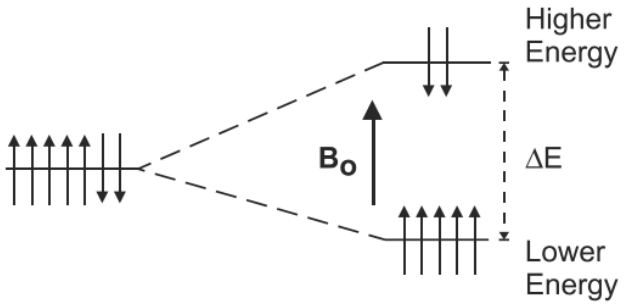

Figure 2.3 Zeeman diagram. In the absence of a magnetic field (left side). In the presence of a magnetic field (right side), the spin up orientation is lower energy and it contains more protons than the higher energy, spin down. The difference in energy ΔE between the two levels is proportional to B_0 [5].

In equilibrium the protons are all out of phase with each other, so the tips of the magnetic moment vectors are evenly spread out around the circles. Since there are so many protons, to make each vector represent the average magnetic moment of a large group of protons all precessing at exactly the same frequency. The vector sum of all these spins is called the net magnetization M_0, which is aligned exactly with the main field B_0 [7].

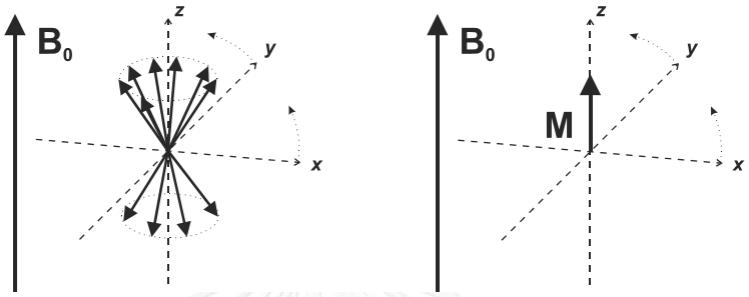

Figure 2.4 Average of many protons produces the net magnetization M_0 [5].

2.1.2 Measuring the net magnetization

In order to detect a signal from protons, the simplest manipulation involves the application of radiofrequency (RF) pulse, also known as an excitation pulse. During the pulse, the protons absorb the energy at a particular frequency. Absorption of the RF energy causes M_0 to rotate away from its equilibrium orientation. The direction of rotation of M_0 is perpendicular to both B_0 and B_1 (Figure 2.5). When the transmitter is turned off, the protons immediately begin to realign themselves and return to their original equilibrium orientation. They emit energy at same frequency as they do so. If a loop of wire (a receiver coil) is placed perpendicular to the transverse plane, the protons induce a voltage in the wire during their precession. This induced voltage, the MR signal, is known as the FID or free induction decay. The FID decays with time as more of the protons give up their absorbed energy through a process known as relaxation (Figure 2.6) [5, 8].

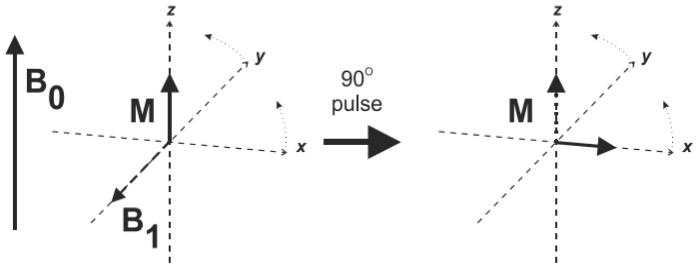

Figure 2.5 Energy absorption, the RF pulse at the resonant frequency can be treated as an additional magnetic field B_1 oriented perpendicular to B_0. When energy is applied at the appropriate frequency, the protons absorb it and M_0 rotates into the transverse plane. The direction of rotation is perpendicular to both B_0 and B_1 [5].

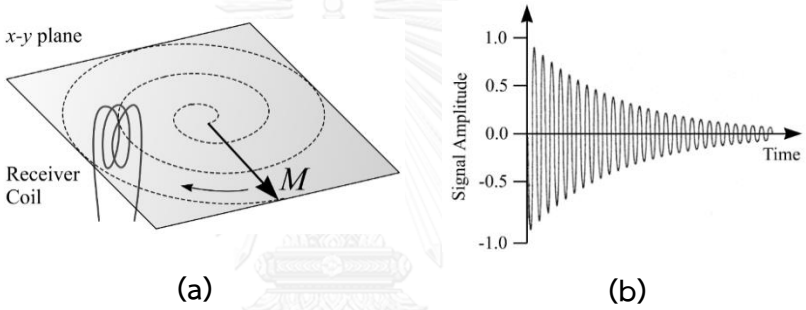

Figure 2.6 (a) After a RF pulse, M_0 lies in the transverse plane and rotates about the z-axis. The component of M_0 in the x-y plane decays over time. (b) An alternating current is induced in the receiver coil [6].

2.1.3 Relaxation process

Relaxation is the process by which protons release the energy that they absorbed from the RF pulse. Relaxation is a fundamental process in MR, as essential as energy absorption, and provides the primary mechanism for image contrast. Two relaxation times can be measured, known as T_1 and T_2. Both times measure the spontaneous energy transfer by an excited proton, but they differ in the final disposition of the energy [5].

T_1 Relaxation

The relaxation time T_1 is the time required for the z component of M_0 to return to 63% of its original value following an excitation pulse. It is also known as the spin-lattice relaxation time or longitudinal relaxation time. This return of magnetization follows an exponential growth process, with T_1 being the time constant describing the rate of growth.

$$M_{z(t)} = M_0\left(1 - e^{\left(-\frac{t}{T_1}\right)}\right) \tag{2.3}$$

where $M_{z(t)}$ is the magnetization at time t, the time after the RF pulse, M_0 is the maximum magnetization at full recovery.

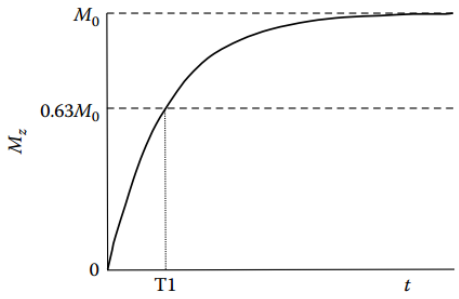

Figure 2.7 The recovery of longitudinal magnetization (M_z) and its relation with the value of T_1 [5].

T_2 Relaxation and T_2* Relaxation

The relaxation time T_2 is the time required for the transverse component of M_0 to decay to 37% of its initial value via irreversible processes. It is also known as the spin–spin relaxation time or transverse relaxation time. T_2 or T_2* relaxation is the process by which this transverse magnetization is lost. The decay of the M_{xy} component is described by an exponential decay with time constant T_2.

$$M_{XY(t)} = M_{XYmax}e^{(-t/T_2)} \tag{2.4}$$

where $M_{XY(t)}$ is the value of M_0 in the x-y plane at time t, M_{Xymax} is the maximum transverse magnetization M_{XY} immediately following the excitation pulse.

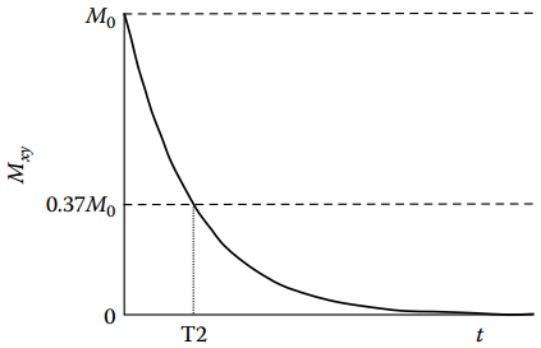

Figure 2.8 The decay of transverse magnetization (M_{xy}) and its relation with the value of T_2 [5].

It was noted earlier that a perfectly homogeneous B_0 field is assumed when considering the T_2 relaxation process. If B_0 is not perfectly homogeneous, then additional dephasing of the spins arises from the inhomogeneities in the magnetic field. The time constant for the decay that results from both intrinsic dephasing and dephasing from field inhomogeneities is T_2*. T_2* is shorter than T_2 (Figure 2.9). The inhomogeneities in B_0 can arise from inherent defects in the magnet itself and susceptibility-induced field distortions from tissue or other materials in the field.

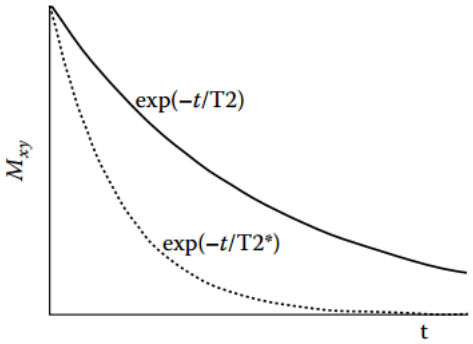

Figure 2.9 A comparison of T_2 decay and the more rapid T_2* decay arising from magnet inhomogeneity [5].

2.1.4 Spatial localization

In order to locate where the acquired signal originates, the magnetic field gradients is used to produce linear variations in one direction only. Three physical gradients are used, one in each of the x, y, and z directions. Each one is assigned to obtain an image: slice selection, readout or frequency encoding, and phase encoding.

The initial step in magnetic resonance imaging is the localization of the RF excitation to a region of space, which is accomplished through the use of frequency-selective excitation in conjunction with a gradient known as the slice selection gradient, G_{SS}. The gradient direction (x, y, or z) determines the slice orientation, whereas the gradient amplitude together with certain RF pulse characteristics determine both the slice thickness and slice position [5].

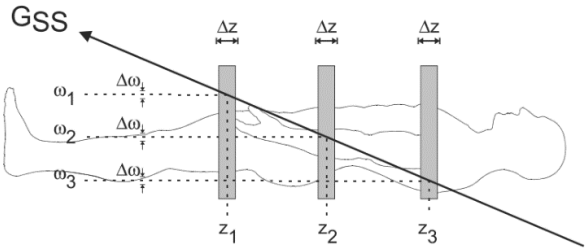

Figure 2.10 Slice selection process. In the presence of a gradient (G_{SS}), the total magnetic field that a proton experiences and its resulting resonant frequency depend on its position. Tissue located at position z_i will absorb RF energy with a unique resonant frequency. The slice thickness Δz is determined by the amplitude of G_{SS} and by the bandwidth of transmitted frequencies [5].

The signal detection portion of the MRI measurement is known as the readout or frequency encoding. In an imaging pulse sequence, the MR signal is always detected in the presence of a gradient known as the readout gradient G_{RO}, which produces one of the two visual dimensions of the image. The readout gradient is applied perpendicular to the slice direction. Under the influence of this new gradient field, the protons begin to precess at different frequencies depending on their position within it.

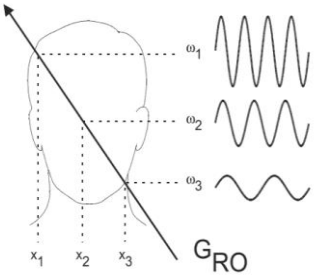

Figure 2.11 Readout process. Following excitation, each proton within the excited volume (slice) precesses at the same frequency. During detection of the echo, a gradient (G_{RO}) is applied, causing a variation in the frequencies for the protons generating the echo signal. The frequency of precession ω_i for each proton depends upon its position x_i [5].

The third direction in an MR image is the phase encoding direction. It is visualized along with the readout direction in an image. The phase encoding gradient, G_{PE}, is perpendicular to both G_{SS} and G_{RO}. Concept of phase encoding will be described in figure 2.12.

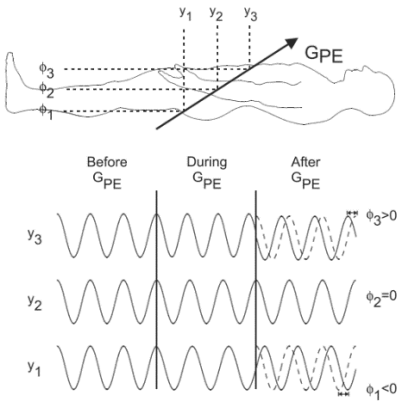

Figure 2.12 Concept of phase encoding. Prior to application of G_{PE}, all protons precess at the same frequency. When G_{PE} is applied, a proton increases or decreases its precessional frequency, depending on its position, y_i. A proton located at $y_i = 0$ (y_2) experiences no effect from G_{PE} ($\Phi_2 = 0$). A proton located at y_3 and y_1 increase and decrease its frequencies while G_{PE} is applied. Once G_{PE} is turned off, the proton precesses at its original frequency, but is ahead of the reference frequency (dashed curve); that is, a phase shift Φ_3 and Φ_1 has been induced [5].

2.1.5 The data matrix (k-space)

A signal is acquired for each phase encoding step, each time with the same frequency encoding gradient applied. The way in which these signals are saved is illustrated in figure 2.13. The value saved at each point in the data matrix represents the amplitude and phase of the signal at that location. The matrix may be referred to as the data matrix, frequency domain representation, or k-space.

It is not usual to display the data matrix itself; instead, the matrix is converted, by performing a two-dimensional Fourier transform, into an MR image that maps the locations of signals in the slice. A two-dimensional transform is required because it is performed on a two-dimensional array and not just on a one-dimensional list of numbers. The Fourier transform allows the signals associated with particular frequencies (x locations) and phases (y locations) to be extracted. By performing slice selection, frequency encoding, and phase encoding, followed by Fourier transformation, an MR image has been produced [9].

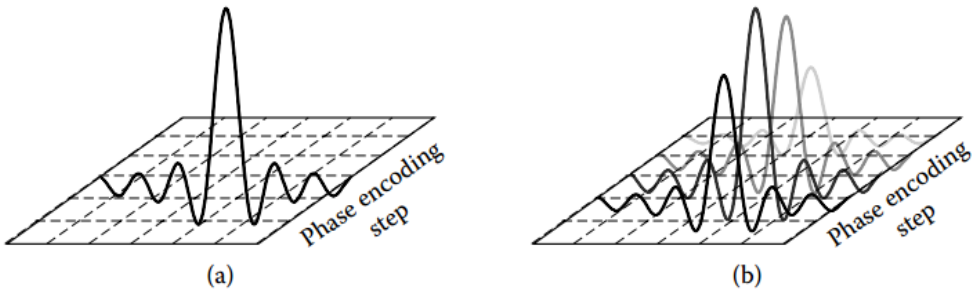

Figure 2.13 (a) The data matrix showing the central positioning of the signal acquired with the phase encoding gradient set to zero. (b) The data matrix with further signals from different phase encoding steps included; each is shown in a different shade of gray. When all the data for an image have been acquired, there will be a signal in the data matrix for every phase encoding step. The value saved at each point in the data matrix represents the amplitude and phase of the signal at that location [9].

2.1.6 Pulse sequences

A pulse sequence is the measurement technique by which an MR image is obtained. It contains the hardware instructions (RF pulses, gradient pulses, and timings) necessary to acquire the data in the desired manner [5].

Spin echo sequences

A commonly used pulse sequence in MR imaging is a spin echo sequence. It has at least two RF pulses, 90° excitation pulse and one or more 180° refocusing pulses that generate the spin echoes. A refocusing pulse is required for every echo produced. There are three types of spin echo sequences are commonly used: standard single echo, standard multi-echo, and echo-train spin echo.

Standard single echo sequences are generally used to produce T_1 weighted images when acquired with relatively short TR and TE (less than 700 ms and 30 ms, respectively).

Standard multi-echo sequences apply multiple 180° refocusing RF pulses following a single excitation pulse. Each refocusing pulse produces a spin echo, each one at a different TE defined by the user. Multi-echo sequences are used to produce proton-density-weighted images using short TE (less than 30 ms) and T_2 weighted images using long TE (greater than 80 ms) when TR is long enough to allow relatively complete T_1 relaxation for most tissues (2000 ms or longer).

Moreover, multi-echo spin echo technique is mostly applied to use for muscle functional MRI. The pulse sequences use multiple 180° RF pulses to generate multiple echoes, in which each echo can be used to create a separate image. Turbo or fast spin echo sequences use the same sequence, but, instead of each echo forming a different image data set, all the echoes are used to create a single image data set at a faster rate, saving imaging time.

The third type of spin echo sequence is known as Turbo spin echo (TSE) or Fast spin echo (FSE). The TSE sequences are similar to standard multi-echo sequences in that multiple 180° pulses are applied to produce multiple echoes following a single excitation pulse. The image is produced using some or all of the measured echoes as

determined by the sequence design. The echo-train length or turbo factor corresponds to the number of echoes used to create the image. The primary advantage of the ETSE technique is that the data collection process is more efficient and the scan time is reduced.

Inversion recovery sequence

Inversion recovery is a spin echo imaging method used for several specific purposes. One application is to produce a high level of T_1 contrast and a second application is to suppress the signals and resulting brightness of fat and fluids. The inversion recovery pulse sequence is obtained by adding an additional 180° pulse to the conventional spin echo sequence. The pulse is added at the beginning of each cycle where it is applied to the longitudinal magnetization carried over from the previous cycle. Each cycle begins as the 180° pulse inverts the direction of the longitudinal magnetization. The regrowth of the magnetization starts from a negative value. The inversion recovery method uses a 90° excitation pulse to produce transverse magnetization and a final 180° pulse to produce a spin echo signal. An additional time interval is associated with the inversion recovery pulse sequence. The time between the initial 180° pulse and the 90° pulse is designated the Time after Inversion (TI). It can be varied by the operator and used as a contrast control [7].

Gradient echo sequences

Gradient echo sequences are a class of imaging techniques that do not use a 180° pulse to refocus the protons. The echo signal is generated only through gradient reversal. Application of imaging gradients induce proton dephasing. Application of a second gradient pulse of the same duration and magnitude but opposite polarity reverses this dephasing and produces an echo known as a gradient echo. Excitation angles less than 90° are normally used. The absence of the 180° RF pulse in gradient echo sequences has several important consequences. The sequence kernel time may be shorter than for spin echo sequence, enabling more slices to be acquired for the same TR. Less total RF power is applied to the patient, so that the total RF energy deposition is lower.

Echo planar imaging sequences

Echo planar imaging (EPI) uses a very different method for data collection. EPI sequences are characterized by a series of gradient reversals in the readout direction. The gradient reversals are performed very rapidly, allowing echo planar images to be acquired in 100–200 ms. The raw data matrix is acquired in a rectilinear, zigzag fashion. Because of the use of gradient echoes, EPI sequences are very sensitive to T_2* effects. In particular, magnetic susceptibility differences will cause image distortions at tissue–bone or tissue–air interfaces, making their use problematic in some anatomical regions. There are two data collection are used in EPI sequences: single-shot and segmented or multi-shot.

Single-shot techniques acquire all phase-encoding steps following a single excitation pulse. Since only one RF pulse is applied per slice position, each image can be acquired with an infinite TR.

Segmented techniques acquire a subset of phase-encoding steps following each excitation pulse. A segmented loop structure with multiple excitation pulses is used to acquire all phase-encoding steps. Segmented EPI can often be performed with standard imaging gradient systems.

The contrast in EPI images is determined by the TE. Each echo is acquired at a different TE, so the TE of the image is referred to as an effective TE. Variations in contrast for EPI sequences are achieved using magnetization-preparation pulses applied prior to the readout period. T_1 weighted images are produced using a 180° inversion RF pulse prior to the excitation pulse. T_2 weighted images can be obtained using a 90°–180°.pair of pulses to produce a spin echo. Spoiled gradient echo EPI sequences use no preparatory pulse and produce T_2* weighted images.

2.1.7 MR equipment

Magnets

The magnet is the basic component of an MRI scanner. Magnets are available in a variety of field strengths, shapes, and materials. All magnet field strengths are measured in units of tesla or gauss (1 tesla = 10,000 gauss). Magnets are usually categorized as low-, medium-, or high-field systems. Low-field magnets have main field strengths less than 0.5 T. Medium-field systems have main magnetic fields between 0.5 and 1.0 T, high-field systems have fields between 1.0 T and 1.5 T, and ultra-high-field systems have fields of 3.0 T or greater [5].

Most MRI systems use a superconducting magnet, which consists of many coils or windings of wire through which a current of electricity is passed, creating a magnetic field of up to 2.0 tesla. Maintaining such a large magnetic field requires a good deal of energy, which is accomplished by superconductivity, or reducing the resistance in the wires to almost zero. To do this, the wires are continually bathed in liquid helium at 452.4 degrees below zero Fahrenheit (269.1 below zero degrees Celsius). This cold is insulated by a vacuum. While superconductive magnets are expensive, the strong magnetic field allows for the highest-quality imaging, and superconductivity keeps the system economical to operate [10].

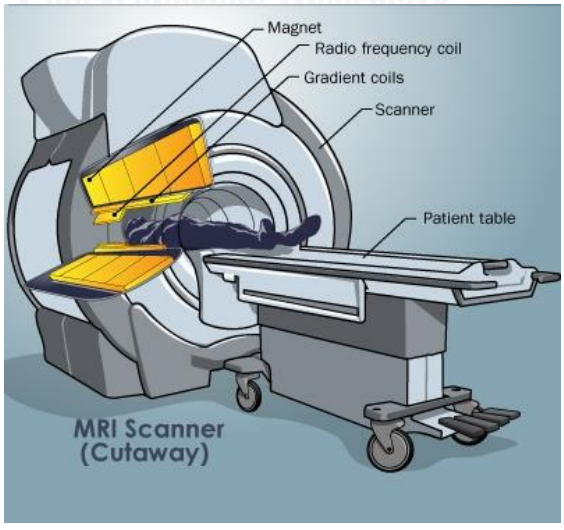

Figure 2.14 The components in a typical MR system [10].

Gradients

The spatial localization of the MR signal requires the use of three orthogonal linear magnetic field gradients. These are generated by gradient coils mounted on a cylindrical former just inside the bore of the magnet. In a standard cylindrical magnet, such as a superconducting system, the direction along the bore is termed the *z* axis, the left–right direction is termed the *x* axis and the top–bottom direction is termed the *y* axis. Although the gradients are oriented in the three orthogonal directions, the gradient magnetic fields themselves are parallel to the main magnetic field B_0. The null point at the center of the gradient coils, and also the center of the magnet, is called the isocenter [11].

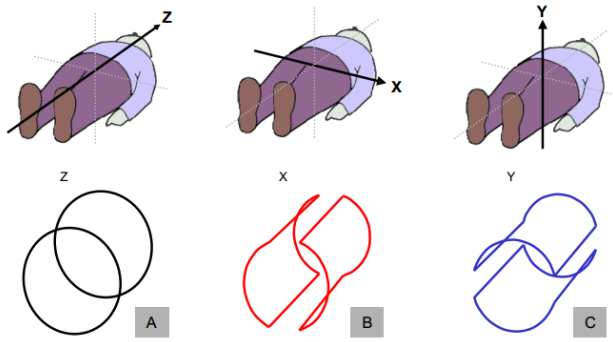

Figure 2.15 Three sets of wires. Each set can create a magnetic field in a specific direction: Z, X or Y. When a current is fed into the Z gradient, then a magnetic field is generated in the Z direction. The same goes for the other gradients [11].

Radiofrequency system

The radiofrequency (RF) system comprises a transmitter, coil and receiver. The purpose of the transmitter is to generate suitably shaped pulses of current at the Larmor frequency. When this current is applied to the coil an alternating B field is produced. The coil will also detect the MR signal from the patient. The frequency-encoding process will result in a narrow range of useful frequencies, e.g. ±16 kHz, centered at the Larmor frequency. It is the function of the receiver to remove, or more correctly demodulate, this ±16 kHz range of interest from the much higher (Larmor frequency) carrier signal [7].

Computer systems

The multi-tasking nature of MR means that it is impractical to control the many processes requiring accurate timing directly from the main or host computer, so many subsystems will have their own microprocessors whose commands can be downloaded from the host. A typical MRI system will have a host computer on which the operator will prescribe the scan in terms of the pulse sequence, its timing and various geometry factors, etc. These parameters will then be converted into commands that are transferred to another microprocessor system, known as the pulse programmer (PP) that controls the hardware. The PP ensures that the RF, gradients and data acquisition are all properly synchronized. Once the data have been acquired, a separate computer system known as the array processor carries out the image reconstruction. The host computer then manages the image display, processing, for example, windowing, hardcopy production, archiving and networking [5].

2.2 The introduction of muscle functional MRI

The muscle functional MRI (mfMRI) is the advent of modern imaging technology offers a variety of approaches for quantifying muscle structure and function. In particular, MRI is frequently used to investigate anatomical information. In addition to its excellent spatial resolution, which permits high-quality imaging of muscle structure, MRI offers a noninvasive method to quantify changes in muscle physiology following the performance of exercise. In particular, signal intensity changes due to increases in the relaxation time (T_2) of tissue water can be measured to indicate exercise-induced activity of muscles [2, 3].

2.2.1 Mechanism of mfMRI

The mfMRI technique is based on an increase in T_2 relaxation time of muscle water following exercise. Specifically, exercise results in a slower decay of the muscle water signal, which causes an enhancement in signal intensity of the activated muscles. As a consequence, activated muscles look brighter on T_2 weighted images when compared to muscles imaged in a resting state (Figure 2.16).

Different studies have been performed to elucidate the underlying physiological mechanism of this shift in T_2 relaxation time [12-14]. The simplest explanation is that the influx of fluid during activity is accompanied by an accumulation of osmolites (phosphate, lactate, and sodium) in the cytoplasm and their presence prolongs the relaxation time of muscle water. The T_2 relaxation time of total muscle water is composed of multiple components, such as protein-bound intracellular water (34%), free intracellular water (49%), and extracellular water (14%), each experiencing a change in their respective T_2 relaxation time. The summed effect of changes in these components results in the net activity-induced increase in T_2. Although all of the components act synergistically to increase overall T_2, it should be clear that activity-dependent increases in T_2 are believed to primarily result from intracellular events.

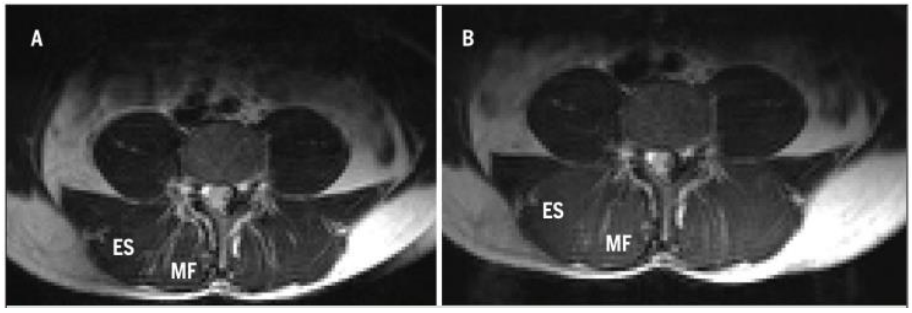

Figure 2.16 T_2 weighted image at rest (A) and following exercise (B) There is an increased signal intensity (brighter) for the m. multifidus (MF) and the m. erector spinae (ES). Although the changes in signal intensity are subtly visible, they are quantifiable using the calculation of T_2 [1].

2.2.2 Measurement protocols

The general mfMRI measurement protocol is that images are acquired at rest (pre-exercise image) and immediately following (post exercise image) a specific exercise. Regions of interest may then be developed for each muscle of interest. Care should be taken to avoid the inclusion of non-muscular tissue (eg, fat, fascia, or blood vessels) in all regions of interest. For each region of interest, the T_2 value may then be calculated and the change in T_2 value recorded from the pre-exercise and post-exercise image is referred to as the "T_2 shift." From these calculations of T_2 shifts, inferences regarding the activity level of specific muscles can be made and compared for different exercise protocols.

The half-life of exercise-induced changes in muscle T_2 has been shown to be approximately 7 minutes [15], which requires the subjects to be accurately placed in the scanner immediately following the performance of the exercise. The time between the end of the exercise and the start of the scan will depend upon what part of the body is imaged and the imaging coils that are used. Future applications might enable patient to perform exercise in the scanner, thereby enabling scanning as soon as exercise is finished. Although there is a fast decay of T_2, full recovery of muscle T_2 is much slower, as T_2 generally remains elevated for approximately 30 minutes following exercise [15, 16]. If the effect of different exercises on muscle activity is to be

evaluated, it is recommended to permit at least 45 minutes of rest between exercise sets, as this allows full recovery of any established T_2 shifts [17].

Different sequences can be used, of which multi-spin echo sequences are mostly applied. During a spin echo pulse sequence, the RF field is applied in 2 pulses: a 90° RF pulse, with a 180° RF pulse to rephrase spins to form an echo. Multi-echo spin echo pulse sequences use multiple 180° RF pulses to generate multiple echoes, in which each echo can be used to create a separate image. Turbo or fast spin echo sequences use the same sequence, but, instead of each echo forming a different image data set, all the echoes are used to create a single image data set at a faster rate, saving imaging time.

2.3 Review of related literature

Fleckenstein JL, Canby RC, Parkey RW, Peshock RM. [18] Publication title: Acute effects of exercise on MR imaging of skeletal muscle in normal volunteers. AJR Am J Roentgenol. 1988; 151(2):231-7. This study evaluated the effects of exercise on MR imaging of skeletal muscle. Imaging of the forearms and/or legs was performed before and after exercise. Exercises included finger flexion and extension, wrist flexion, ankle plantar flexion, and great toe extension. Individual muscles were frequently indistinguishable on pre-exercise scans.

The result showed active and inactive muscles could be clearly distinguished. Exercise results in signal-intensity changes that are useful in showing individual muscle. The changes in signal intensity correlate weakly with the level of exertion. The activated muscles were most apparent on spin-echo scans having longer TRs and TEs, so the contrast was greatest on T_2-weighted sequences (Figure 2.17). They found at the first that exercise leads to transient increases in skeletal muscle intensity related to increases in tissue relaxation times and spin density.

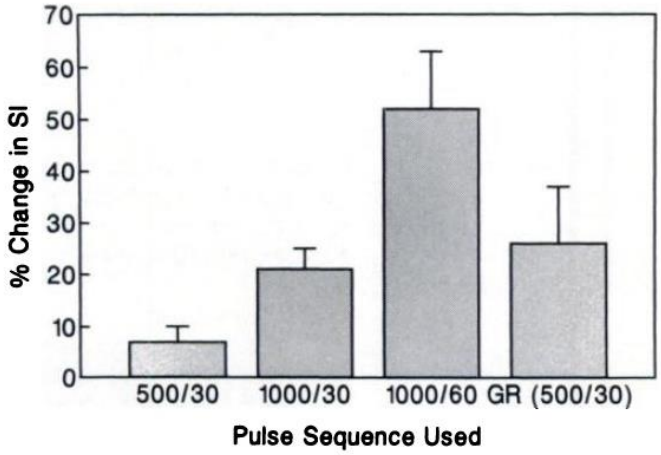

Figure 2.17 Percentage increase in signal intensity (SI) of flexor digitorum profundus (FDP) immediately after intense handgrip is shown for different pulse sequences [18].

Fisher MJ, Meyer RA, Adams GR, Foley JM, Potchen EJ. [15] Publication title: Direct relationship between proton T_2 and exercise intensity in skeletal muscle MR images. Invest Radiol. 1990; 25(5):480-5. They studied the effect of force generation during exercise on muscle T_2 values and examined the effects of extracellular fluid volume (ECV) expansion on muscle T_2 values. The axial mid-calf images were collected before and after exercise using a standard spin echo sequence. Exercise consisted of three consecutive of ankle dorsiflexion against graded loads.

This investigation demonstrates that T_2 values for the dorsiflexors significantly increased after exercise, however a direct relationship between increases in T_2 and in ECV after exercise was not established. The contrast enhancement among muscle after exercise in T_2-weighted MR images is dependent on the average force generated by the muscle during exercise. This study suggested that the prolongation in T_2 relaxation time could be used as a quantitative measurement for muscle activity.

Akima H, Takahashi H, Kuno SY, Katsuta S. [19] Publication title: Co-activation pattern in human quadriceps during isokinetic knee-extension by muscle functional MRI. Eur J Appl Physiol. 2004; 91(1):7-14. This study investigated the activation patterns of individual muscles and neuromuscular compartments of the quadriceps femoris during knee-extension exercises.

This study demonstrated that at least two strategies are applied for force production in the human quadriceps femoris. The co-activation of specific pairs of individual muscles and regional-specific activation in neuromuscular compartments in the rectus femoris. In conclusion, the exercise-induced changes in MR images were influenced not only by workload and exercise duration but also by the specific type of exercise (Figure 2.18).

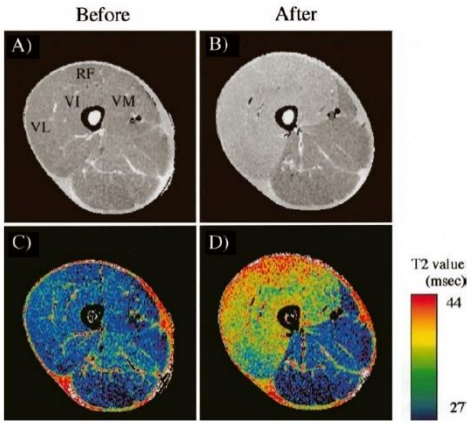

Figure 2.18 Representative T_2 weighted images (A, B) and T_2 mapping images (C, D) of the right thigh before and after knee extension exercise. Specific exercise can be distinguished active and inactive muscle in muscle T_2 mapping images [19].

Tawara N, Nitta O, Itoh A. [20] Publication title: Comparison of pulse sequences for T_2 measurement of human skeletal muscle. Jpn J Magn Reson 2008; 28:25-34. This study investigated which differences in pulse sequence affect the transverse relaxation (T_2) decay curve and T_2 itself. They compared multiple-spin-echo (MSE) and spin-echo echo-planar-imaging (SE-EPI) sequences of magnetic resonance (MR) imaging. T_2 measurements were taken in 2 kinds of uniform phantoms and in the right gastrocnemius (GA) muscle of a human.

In the 2 phantoms, the T_2 decay curves from MSE and SE-EPI were comparable; each phantom showed a single T_2. In the right GA, the T_2 decay curves from SE-EPI and MSE sequences were dissociated when echo time (TE) was high. These results suggested that the dephasing from the external magnetic field inhomogeneity in tissue affected the sampling of the k-space. Moreover, the image contrast from the SE-EPI sequence revealed a combination of T_2 decay mixed with T_2* decay. In conclusion, the SE-EPI may be the fastest available MR imaging technique for T_2 measurement. However, that the image contrasts of the MSE and SE-EPI sequences are not strictly equal in humans, though they have been confirmed to be similar. Thus, the use of the SE-EPI sequence confirmed that the TE of the section not influenced by T_2* decay is under than 75 ms.

Tawara N, Nitta O, Kuruma H, Niitsu M, Itoh A. [21] Publication title: T_2 mapping of muscle activity using ultrafast imaging. Magn Reson Med Sci. 2011;10(2):85-91.This study evaluated the feasibility of T_2 mapping of muscle activity using ultrafast imaging technique, called fast-acquired mfMRI (fast-mfMRI), to reduce image acquisition time and compared with conventional technique (Multiple spin echo) which requires several minutes for acquisition. The current method uses 2 pulse sequences, SE-EPI images are used to calculate T_2, and TrueFISP images are used to obtain morphological information. To calculate muscle T_2 relaxation time using mono-exponential linear least-squares regression methods.

This study presented fast-mfMRI with acquisition time one-twelfth that of the previously used method. The scan time of the fast-mfMRI (22 s) is much shorter than that of mfMRI (4 min 20 s). However this study does not examine the imaging conditions, especially TR which related with the scan time, for calculating T_2, even though precision of T_2 calculated by mono-exponential linear least-squares regression is influenced by the signal-to-noise ratio (SNR).

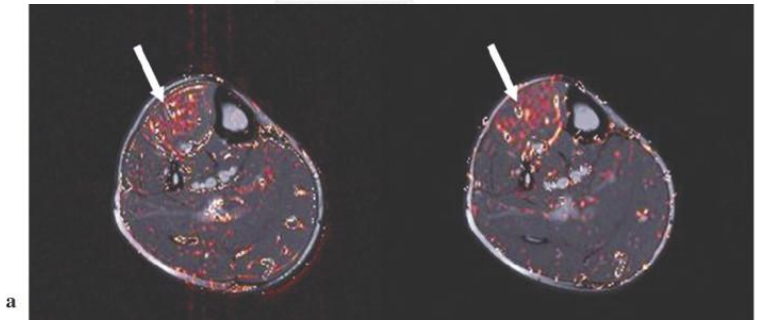

Figure 2.19 Fusion images [fast-mfMRI]) produced from multiple spin-echo (MSE) (a) and spin-echo echo-planar imaging (SE-EPI) images (b). The bright areas on both images agree with each other (arrows). Areas of deep red color indicated where muscle activation greatest [21].

CHAPTER 3

RESEARCH METHODOLOGY

3.1 Research design

This study is an experimental study.

3.2 Research design models

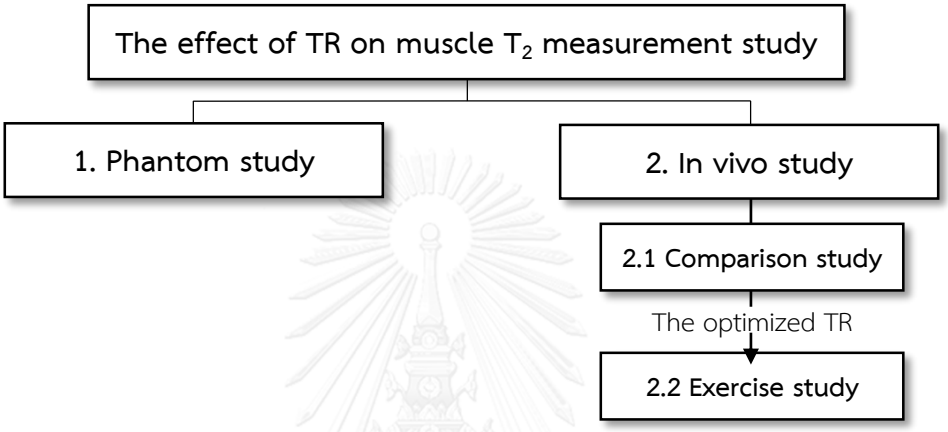

Figure 3.1 Overview of research design model.

3.2.1 Phantom study

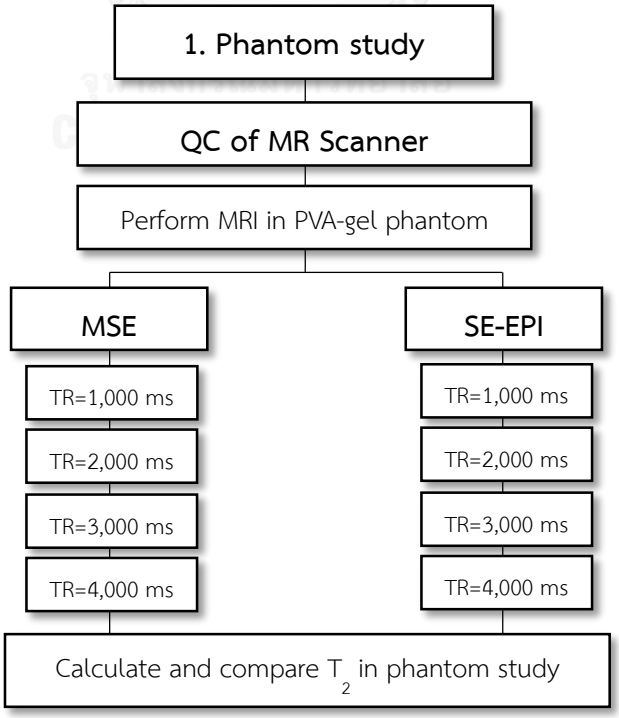

Figure 3.2 Research design model of phantom study.

3.2.2 In vivo study

3.2.2.1 Comparison study

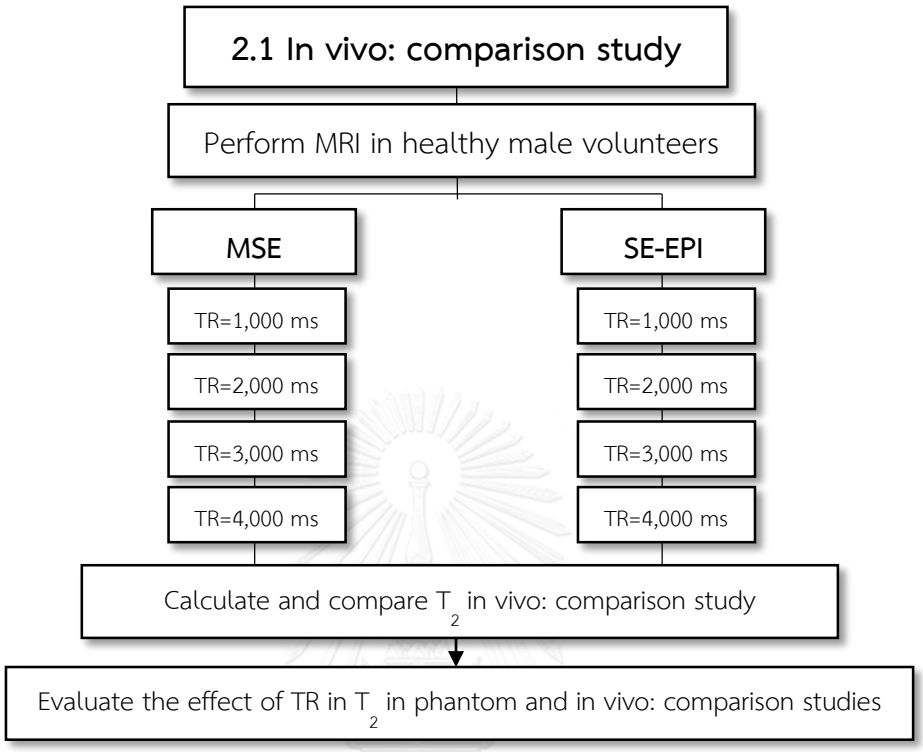

Figure 3.3 Research design model of in vivo: comparison study.

3.2.2.2 Exercise study

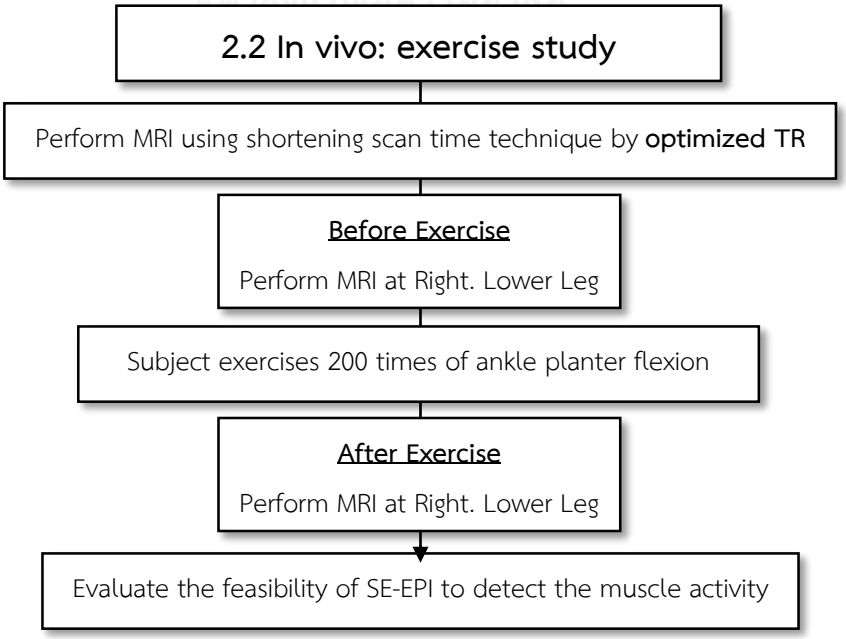

Figure 3.4 Research design model of in vivo: exercise study.

3.3 Conceptual framework

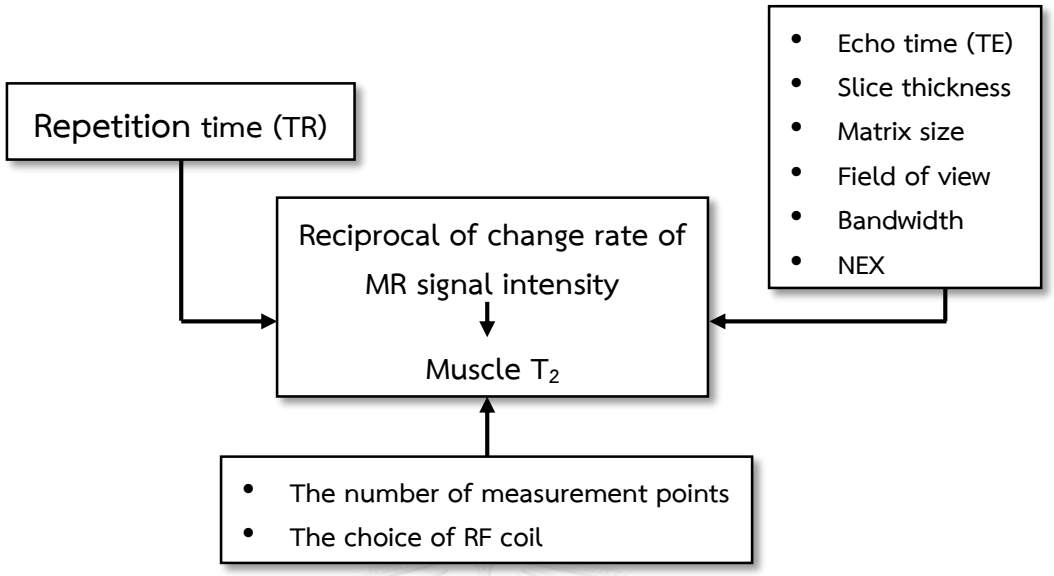

Figure 3.5 Conceptual framework.

3.4 Research questions

3.4.1 Primary research question

What is the effect of repetition time (TR) on decreasing scan time for muscle T_2 measurement comparing multiple spin echo (MSE) to spin echo-echo planar imaging (SE-EPI) at 1.5 Tesla MRI?

3.4.2 Secondary research question

What is the feasibility of shortening scan time technique for muscle T_2 measurement to detect the muscle activity that induced by exercise?

3.5 The sample

3.5.1 Target population

The healthy male volunteers age 18-35 years, no history of muscle disorders and can exercise as defined while MRI examination recruited based on the simple random sampling.

3.5.2 Sample population

The healthy male volunteers recruited based on the following eligible criteria.

3.5.3 Eligible criteria

3.5.3.1 Inclusion criteria

- Healthy male subject ages between 18-35 years.
- No clinically important abnormal physical finding.
- No history of muscle disorders or muscle injury.
- Competent and willing to give inform consent.

3.5.3.2 Exclusion criteria

- The subject who has metal embedded in the body.
- The subject who has claustrophobia and cannot perform MRI.
- The subject who is unable to exercise as defined.

3.5.4 Sample size determination

The sample population in each group was determined by the formula [22].

$$N = \frac{2(z_\alpha + z_\beta)^2(1+(n-1)\rho)}{n[(\mu_1 - \mu_2)/\sigma]^2} \quad (3.1)$$

- N is number of subjects in each of two groups.
- σ^2 is the assumed common variance in the two groups.
- $\mu_1 - \mu_2$ is the difference in means of the two groups.
- n is the number of time points.
- ρ is the assumed correlation of the repeated measures.

$$N = \frac{2(1.96+1.282)^2(1+(4-1)0.6)}{4[(5)/2.5]^2} = \frac{21.0211 \times 2.8}{16} = 3.678 \cong 4 \quad (3.2)$$

- Z_α = 1.96 (2-tailed 0.05 hypothesis test)
- Z_β = 1.282 (power = 0.9)
- $\mu_1 - \mu_2$ = 5 ms (the least difference in means between the two groups that make the difference [21])
- Σ = 2.5 (assumed common standard deviation (S.D.) [23])
- n = 4 time points (TR 1,000, 2,000, ..., 4,000 ms)
- ρ = 0.6 (assumed correlation of the repeated measures)

Need approximately 4 subjects in each group, total sample size = 4x2 = 8.

3.6 Materials

3.6.1 MRI 1.5 Tesla whole body scanner, Siemens, MAGNETOM Aera

Figure 3.6 MRI 1.5 Tesla (MAGNETOM Aera; Siemens AG, Erlangen, Germany).

MRI 1.5 Tesla, with 70 cm open bore and in combination with ultra-short system design, digital coil and auto calibration, installed at King Chulalongkorn Memorial Hospital in 2012, is used in this study.

3.6.2 The 20-channel head/neck phase array coil

Figure 3.7 The 20-channel head/neck phase array coil.

The 20-channel head/neck coil is used for quality control of MR scanner. The coil design with 20 integrated pre-amplifiers, two rings of 8 elements each and one ring with 4 elements, combined coil for head and neck examination for optimized workflow, upper coil part easy removable, lower coil part usable without upper part for highly claustrophobic patients.

3.6.3 ACR MRI accreditation phantom

Figure 3.8 ACR MRI accreditation phantom.

The ACR MRI accreditation phantom is used for quality control of MR scanner. The phantom is made of acrylic plastic, glass and silicone rubber. The inside length is 148 mm; the inside diameter is 190 mm. It is filled with the solution of nickel chloride and sodium chloride: 10 mM $NiCl_2$ and 75 mM NaCl. The outside of the phantom has the words “NOSE” and “CHIN” etched into it as an aid to orienting the phantom for scanning. Several structures are designed inside the phantom to facilitate a variety of scanner performance tests.

3.6.4 CP extremity coil

Figure 3.9 CP extremity coil.

The circular polarized coil (CP Extremity Coil) is used for phantom and in vivo studies. The coil is transmit/receive coil with 2 integrated preamplifiers. Upper coil part is removable. Holder allows off-center positioning to keep knee or foot which is not under examination in a comfortable position.

3.6.5 PVA-gel phantom

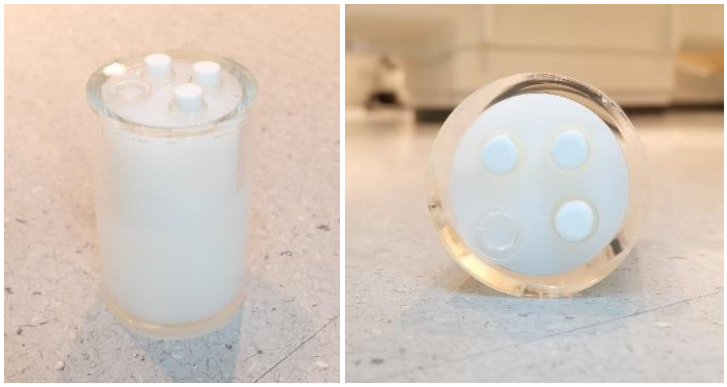

Figure 3.10 PVA-gel phantom (NIKKO FINES INDUSTRIES Co.,Ltd, Tokyo, Japan).

A PVA gel phantom (T_2 approximately 90 ms) is used for phantom study. It is constructed from polyvinyl alcohol gel solution. MRI parameter (^1H density, T_1, T_2) is close to human soft tissue. The physical characteristics is appropriate of long-term stability and can be used as a reference of human soft tissue.

3.6.6 Siemens Syngo workstation software

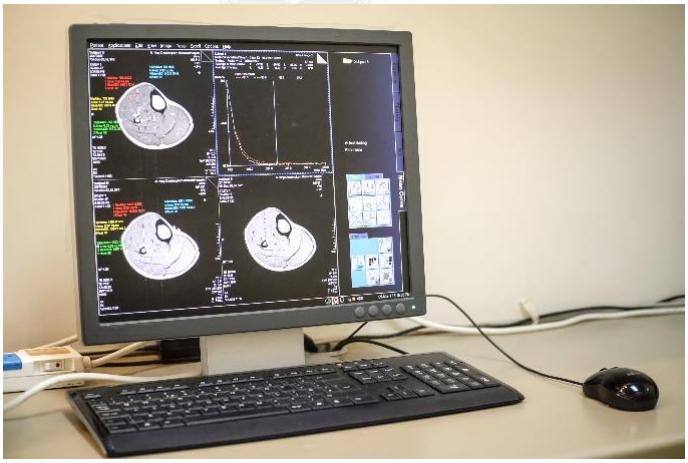

Figure 3.11 Siemens Syngo workstation software.

The software is used for measuring signal intensities on each image in order to generate T_2 relaxation curve and calculate muscle T_2. The software include features for routine and advanced post-processing, draw ROI and quantify means signal intensities, method of quantitative tissue characterization.

3.7 Methods

3.7.1 Quality control of MRI scanner

The quality control of MRI 1.5 Tesla was performed following ACR MRI quality control manual (2015) [24]. The QC procedures were:

- Geometric accuracy
- High contrast spatial resolution
- Slice thickness accuracy
- Slice position accuracy
- Image intensity uniformity
- Percent signal ghosting
- Low contrast object detectability

3.7.2 Phantom study

a. Position a PVA-gel phantom in CP extremity coil at the center alignment of the magnetic field.

b. Perform the multiple spin echo (MSE) and spin echo-echo planar (SE-EPI) sequences using 4 conditions of TRs; TR 1,000, 2,000, 3,000 and 4000 ms. Set other parameters as in table 3.1.

c. Measure the signal intensities on each image in order to generate T_2 relaxation curve and calculate T_2 between MSE and SE-EPI.

Table 3.1 Pulse sequences parameters of phantom and in vivo: comparison studies.

Parameter protocol	MSE	SE-EPI
Repetition time (TR) (ms)	4 TRs (1,000, 2,000, ..., 4,000 ms)	4 TRs (1,000, 2,000, ..., 4,000 ms)
Echo time (TE) (ms)	25 TEs (15, 30, 45, ..., 390 ms)	25 TEs (29, 30, 45, ..., 390 ms)
Matrix size	256×256	256×256
Flip angle (deg)	N/A	90°
Bandwidth (Hz/Px)	N/A	1392
Acquisition time	4:20, 8.36, 12.53, 17.10 min	1, 2, 3, 4 second per echo
Slice thickness (mm)	5	5
FOV (mm^2)	200x200	200x200
Number of Excitation	1	1

3.7.2 In vivo study

3.7.2.1 Comparison study

Eight healthy male volunteers (mean age±SD and range of 28.87±3.98 (25.3–35.7) years; mean height±SD and range of 171.13±5.20 (163-180) cm; mean weight±SD and range of 65.19±7.03 (54.5-74) kg) were performed MR imaging at the level of intermediate of calf. All subjects were given written informed consent prior to the study.

a. Position the right lower leg of male subject in CP extremity coil at the center alignment of the magnetic field.

b. Perform transverse MR Images at the intermediate level of calf using the same pulse sequences acquisition parameters as in table 3.1.

c. Calculate and compare T_2 relaxation curve and T_2.

d. Evaluate the effect of TR on muscle T_2 in phantom and in vivo: comparison studies and obtain the optimized TR.

3.7.2.2 Exercise study

To evaluate the feasibility of fast-mfMRI technique to detect muscle activity, 2 pulse sequences were used. SE-EPI which optimized TR was used to calculate T_2 and TrueFISP images were used to obtain morphological information. Set the pulse sequences acquisition parameters as in table 3.2.

a. Before exercise

Position the right lower leg of male subject in CP extremity coil at the center alignment of the magnetic field and perform transverse MR images at the intermediate level of calf using 2 pulse sequences, SE-EPI by optimized TR and TrueFISP sequences.

b. Exercise

Subjects lying supine on MRI examination table and exercise 200 times of 90° of ankle plantar flexion using a training-gum-belt following an electric metronome 3 seconds per time.

c. After exercise

Perform MRI immediately using the same pulse sequences.

Table 3.2 Pulse sequences parameters of in vivo: exercise study.

Parameter protocol	TrueFISP	SE-EPI
Repetition time (TR) (ms)	5.36	1000
Echo time (TE) (ms)	2.68	5 TEs (29, 30, 45, 60, 75 ms)
Matrix size	256×256	256×256
Flip angle (deg)	70°	90°
Bandwidth (Hz/Px)	501	1392
Acquisition time (sec)	3 sec	1 sec per echo
Slice thickness (mm)	5	5
FOV (mm^2)	200x200	200x200
Number of excitation	1	1

3.8 Data analysis

3.8.1 Data analysis of phantom and in vivo: comparison studies

The region of interests (ROIs) were placed on PVA-gel image at the center core of the image and muscle images at tibialis anterior muscle [TA] by avoiding flow vessel area. ROIs were mapped at same area of phantom and muscle images in order to measure signal intensities (Figure 3.12).

T_2 and T_2 relaxation curves were analyzed using mono-exponential linear least-squares methods of TE = 30, 45, 60, 75 ms. The first image (TE = 15 ms in MSE, TE = 29 ms in SE-EPI) was excluded from the analysis to minimize saturation effects [20].

T_2 are presented as mean ± standard deviation. T_2 between each TRs were compared by T_2 relaxation curve and T_2.

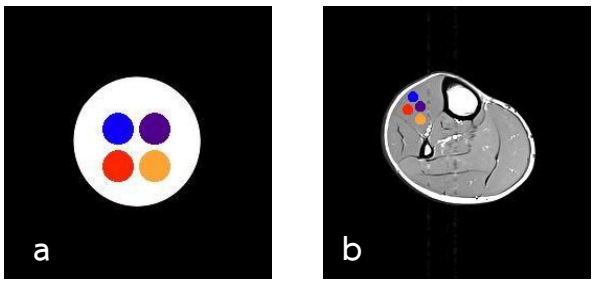

Figure 3.12 ROIs are placed on PVA-gel image (a) and axial MR image of right leg at tibialis anterior muscle [TA] (b).

3.8.2 Data analysis of in vivo: exercise study

ROIs of the muscle were determined in the area of each muscle at rest and after exercise at tibialis anterior muscle [TA] and gastrocnemius muscle [GA] (Figure 3.13). T_2 were analyzed using mono-exponential linear least-squares methods of TE = 30, 45, 60, 75 ms [20].

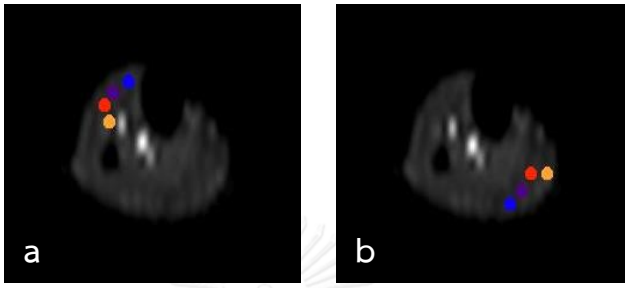

Figure 3.13 ROIs are placed on muscle image at tibialis anterior muscle (a) and gastrocnemius muscle images (b).

3.9 Statistical analysis

3.9.1 Statistical analysis of phantom and in vivo: comparison studies

Reference form the previous studies [25, 26] concluded that relaxation times (T_1 and T_2) within the majority of the biologic range can be estimated by MRI with an overall accuracy of 5 to 10 percent. The wide spread in relaxation time measurement is due to real variations and not a lack of precision [27].

In this study, the results of T_2 comparison exceeding 10 percent of the T_2 were assumed to be significantly different.

3.9.2 Statistical analysis of in vivo: exercise study

The paired t-test was used to determine the statistical difference between the T_2 at rest and after exercise; $P<0.05$ was considered significant.

3.10 Outcome measurement

Independent variables: Repetition time (TR)

Dependent variables: Signal intensity, T_2

(T_2 are calculated from reciprocal of change rate of signal intensity.)

3.11 Expected benefit

The effect of TR on decreasing scan time for muscle T_2 measurement was studied in the research. MSE and SE-EPI were used by various TR in order to obtain the optimized TR for reducing scan time.

The second purpose of the research is to evaluate the feasibility of shortening scan time technique to detect muscle activity. The innovative technique with optimized TR was proposed for muscle T_2 measurement to reduce scan time dramatically and can be applied to the trunk muscle to detect muscle activity in single breath-hold.

3.12 Ethical consideration

The researcher is ethical conduct research in these three verses, including the respect for the individual (Respect for person) by make information sheet for research participants to receive adequate information about the study before signing a consent form and have the right to refuse participation at any time. Researchers will maintain the confidentiality of the volunteer records in no identifiable data of participants. Potential risks to the participants are protected (Beneficence / Non-maleficence) by a check list for screening before and after perform MRI and there is the protective equipment to avoid skin contact with the coil directly and a device used to reduce noise. The Justice (Justice) is a clear entry and exit criteria. The data is collected without discrimination on race or socioeconomic status. The healthy subject will generally be recruited based on the following inclusion and exclusion criteria. Inclusion criteria: Healthy male subject age is between 18-35 years old, no clinically important abnormal physical finding, do not exercise for at least one week, no history of muscle disorders or muscle injury, able to communicate and competent and willing to give inform consent. Exclusion criteria: The subjects who have taken the nutrient to strengthen the muscle, has metal embedded in the body, has claustrophobia and cannot perform MRI, unable to exercise as defined and unable communicate.

This MRI study was performed in phantom and in healthy male volunteers on 1.5 Tesla MR Scanner at King Chulalongkorn Memorial Hospital. The research had been approved by Ethical Committee of Faculty of Medicine, Chulalongkorn University.

3.13 Limitation

Many literatures, not only report single-component muscle T_2 but also multi-component muscle T_2. This study is assumed to be single-component muscle T_2, we used the mono-exponential linear least-squares method for calculation of muscle T_2 relaxation time and cannot assess the muscle activity in the case of multi-component muscle T_2.

CHAPTER 4

RESULTS

4.1 Quality control of MRI scanner

The quality control of 1.5 Tesla MRI system was performed by following the ACR manual (2015) [24]. The results of geometric accuracy, high contrast spatial resolution, slice thickness accuracy, slice position accuracy, image intensity uniformity, percent signal ghosting and low contrast object detectability are shown in Appendix B. The report of MRI system performance test is shown in table 4.1.

Table 4.1 Report of MRI 1.5 Tesla performance test.

LOCATION	King Chulalongkorn Memorial Hospital
DATE	May 25, 2016
MANUFACTURER	Siemens Healthcare
MODEL	MAGNETOM Aera 1.5 Tesla
SERIES NUMBER	52058
SOFTWARE VERSION	Syngo MR E 11
Geometric accuracy	Pass
High contrast spatial resolution	Pass
Slice thickness accuracy	Pass
Slice position accuracy	Pass
Image intensity uniformity	Pass
Percent signal ghosting	Pass
Low contrast object detectability	Pass

4.2 Phantom study data

The MR images were generated using multiple spin echo (MSE) and spin echo-echo planar imaging (SE-EPI) sequences by the differences TRs and TEs (Table 3.1). To measure the signal intensity, four ROIs were placed at the center core of PVA-gel images on each image. T_2 relaxation curve was presented as the plot of signal intensity and echo time. T_2 relaxation time was calculated using mono-exponential linear least-squares regression methods. T_2 relaxation curves of PVA-gel phantom are shown in figure 4.1 for MSE, figure 4.2 for SE-EPI and figure 4.3 for the comparison of T_2 relaxation curve between MSE and SE-EPI. T_2 of phantom study are shown in table 4.2 and 4.3.

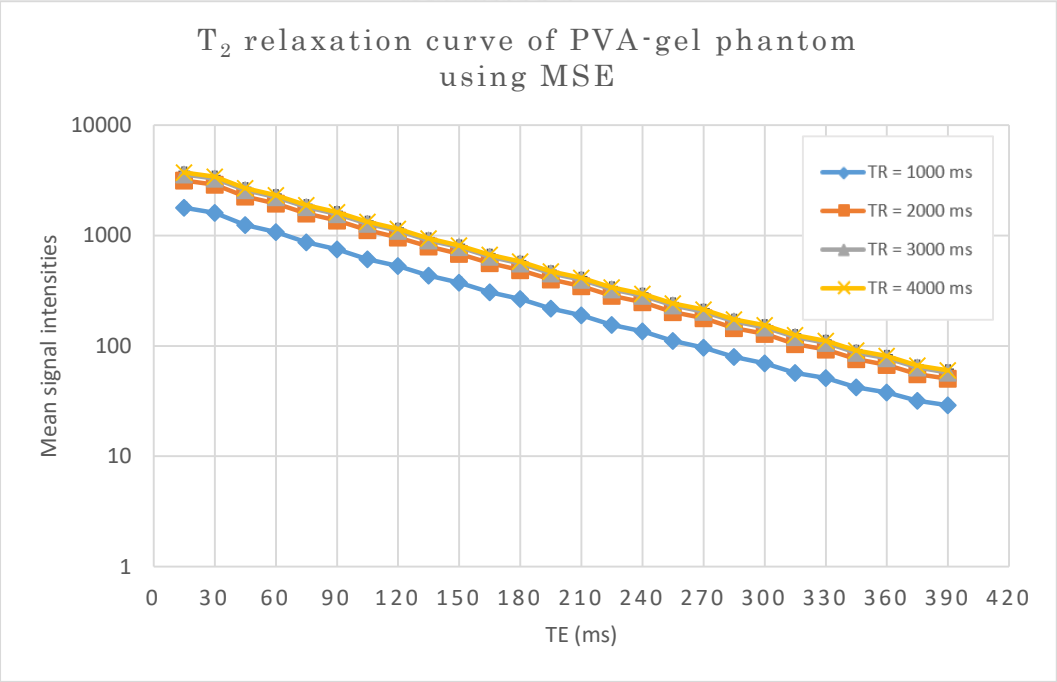

Figure 4.1 T_2 relaxation curve of PVA-gel phantom using MSE.

From figure 4.1, MR signal of MSE increases with increasing TR. The signal intensity curve of TR 1,000 ms is lower than the other TR's signals. The relaxation curve when TR is 2,000 ms or more, tended to show approximately the same MR signal.

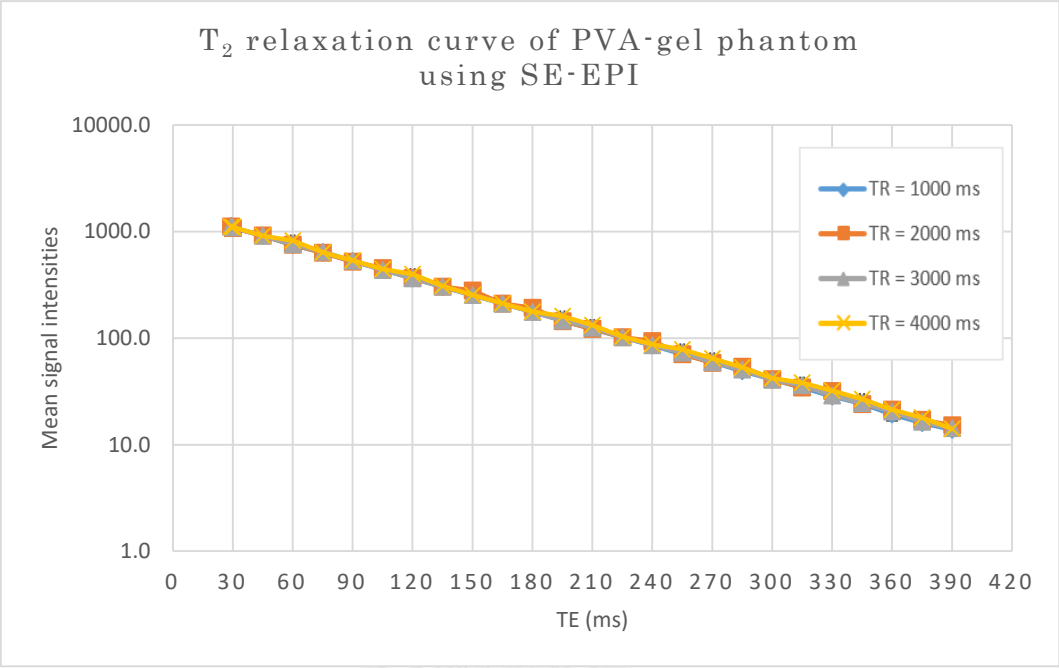

Figure 4.2 T_2 relaxation curve of PVA-gel phantom using SE-EPI.

From figure 4.2, T_2 relaxation curve of all TR show approximately the same MR signal.

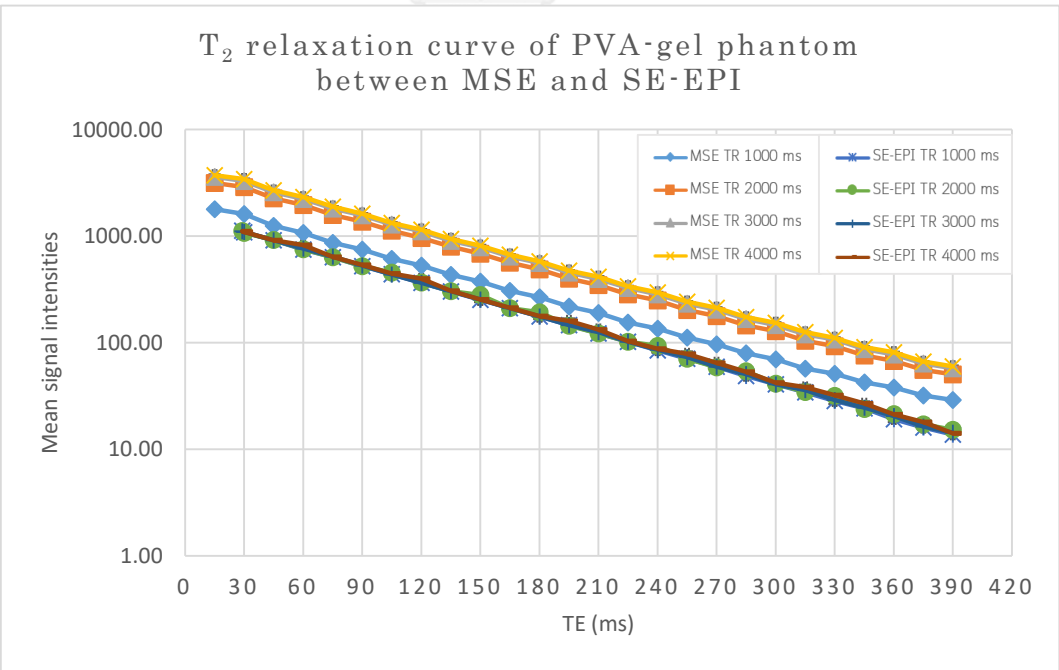

Figure 4.3 T_2 relaxation curve of PVA-gel phantom between MSE and SE-EPI.

From figure 4.3, comparison of T_2 relaxation curve between MSE and SE-EPI. All MR signals of SE-EPI are lower than the signals by MSE.

Table 4.2 T_2 of phantom study using MSE and SE-EPI by variation of TR.

Phantom study	ROIs	T_2 (ms)			
		TR 1,000 (ms)	TR 2,000 (ms)	TR 3,000 (ms)	TR 4,000 (ms)
MSE	1	76.04	78.06	78.67	78.71
	2	75.90	77.98	78.42	78.58
	3	75.74	78.09	78.74	79.23
	4	75.59	77.82	78.58	78.89
	Means±SD	75.82±0.20	77.99±0.12	78.60±0.14	78.85±0.28
SE-EPI	1	82.54	84.04	85.52	83.49
	2	82.57	83.43	85.49	84.08
	3	82.56	83.55	85.00	83.34
	4	82.12	83.36	84.69	83.21
	Means±SD	82.45±0.22	83.60±0.31	85.18±0.40	83.53±0.38

Table 4.3 T_2 of phantom study using MSE and SE-EPI versus the percent difference values in each TR and sequences.

Sequences	T_2 (ms)				% Difference
	TR 1,000 ms	TR 2,000 ms	TR 3,000 ms	TR 4,000 ms	
MSE (ms)	75.82±0.20	77.99±0.12	78.60±0.14	78.85±0.28	4.54
SE-EPI (ms)	82.45±0.22	83.60±0.31	85.18±0.40	83.53±0.38	3.99
% Difference	8.91	7.47	8.68	6.57	

From the table 4.3, T_2 of PVA-gel phantom between MSE and SE-EPI in each TR are compared. The results of T_2 comparison exceeding 10 percent difference are assumed to be significant difference [25]. All T_2 are not significantly different between the parameter TR and sequences.

4.3 In vivo study data

4.3.1 Comparison study data

The signal intensities from the muscle MR images of 8 healthy male volunteers (mean age±SD and range 28.87±3.98 (25.3–35.7) years; mean height±SD and range 171.13±5.20 (163-180) cm; mean weight±SD and range 65.19±7.03 (54.5-74) kg) were measured by determining the ROIs in the area of tibialis anterior muscle [TA] by avoiding flow vessel area. T_2 relaxation curves are plotted as mean signal intensities versus echo time and presented in figure 4.4 for MSE, figure 4.5 for SE-EPI and figure 4.6 for the comparison of T_2 relaxation curve between MSE and SE-EPI. T_2 of in vivo: comparison study are shown in table 4.4 and 4.5.

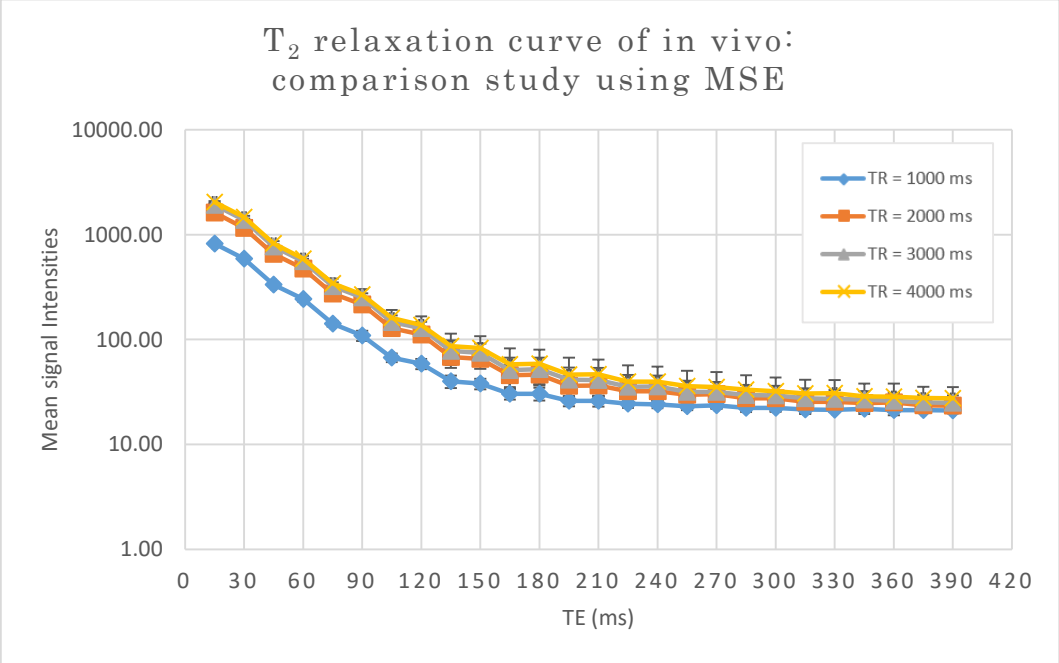

Figure 4.4 T_2 relaxation curve of in vivo: comparison study using MSE.

From figure 4.4, the results of in vivo: comparison study is in line with phantom study. MR signal of TR 1,000 ms is lower than the other TR's signals. The relaxation curve of TR 2,000 ms or more is likely to be the same MR signal.

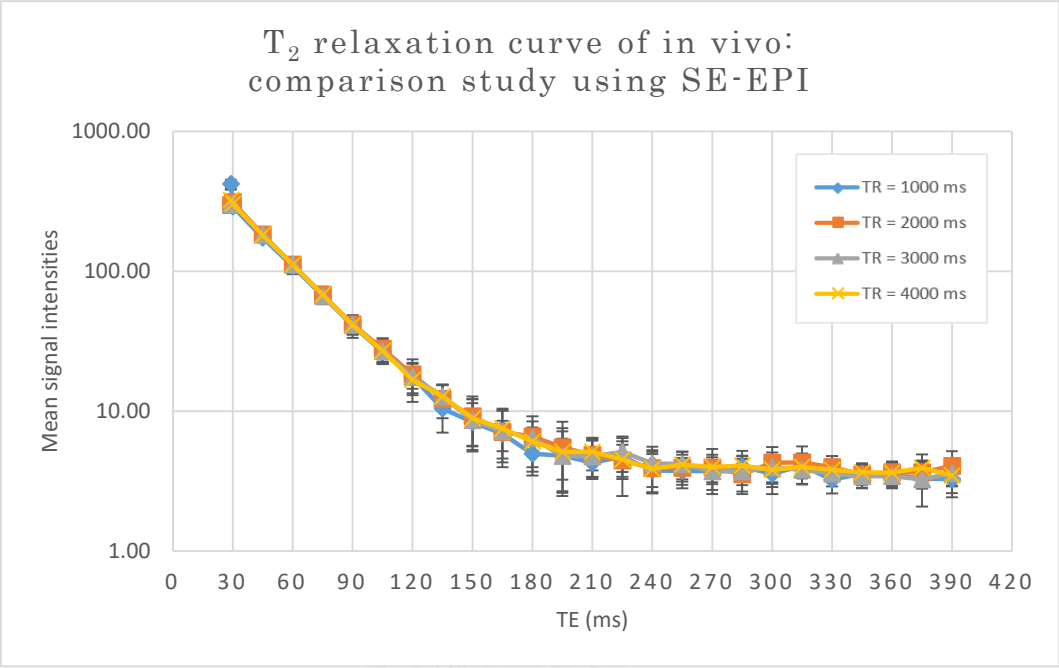

Figure 4.5 T_2 relaxation curve of in vivo: comparison study using SE-EPI.

From figure 4.5, the SE-EPI relaxation curve of all TR is almost as same.

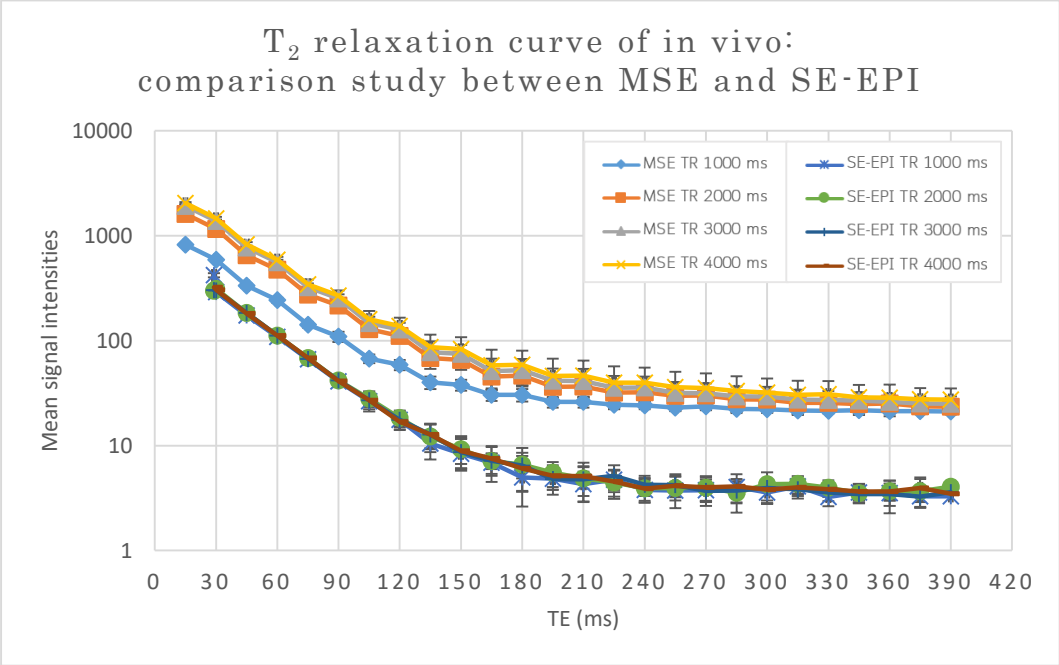

Figure 4.6 T_2 relaxation curve of in vivo: comparison study between MSE and SE-EPI.

From figure 4.6, comparison of T_2 relaxation curve between MSE and SE-EPI. All MR signals of SE-EPI are lower than the signals by MSE as in the phantom study.

Table 4.4 T_2 of in vivo: comparison study from 8 healthy male volunteers using MSE and SE-EPI by four condition of TR.

Sequences	Subject No.	T_2 (ms)			
		TR 1,000 (ms)	TR 2,000 (ms)	TR 3,000 (ms)	TR 4,000 (ms)
MSE	1	33.24	34.83	33.61	35.09
	2	31.30	30.54	30.10	29.92
	3	33.70	33.43	34.18	34.98
	4	31.65	30.37	29.95	30.14
	5	32.47	32.29	31.96	32.53
	6	32.28	31.66	31.55	31.89
	7	32.52	31.94	31.91	32.39
	8	32.98	32.47	31.98	31.55
	Means±SD	32.52±0.80	32.19±1.46	31.90±1.48	32.31±1.93
SE-EPI	1	33.97	33.12	31.64	32.51
	2	29.09	31.26	28.40	28.73
	3	30.69	30.81	31.58	31.88
	4	30.96	27.69	29.02	29.79
	5	31.18	30.72	30.16	30.73
	6	30.48	30.12	29.79	30.28
	7	30.83	29.84	30.14	30.67
	8	29.22	28.06	28.28	28.29
	Means±SD	30.80±1.50	30.20±1.74	29.88±1.25	30.36±1.44

Table 4.5 T_2 of in vivo: comparison study using MSE and SE-EPI versus the percent difference values in each TR and sequences.

Sequences	T_2 (ms)				% Difference
	TR 1,000 (ms)	TR 2,000 (ms)	TR 3,000 (ms)	TR 4,000 (ms)	
MSE (ms)	32.52±0.80	32.19±1.46	31.90±1.48	32.31±1.93	1.92
SE-EPI (ms)	30.80±1.50	30.20±1.74	29.88±1.25	30.36±1.44	3.03
% Difference	5.43	6.38	6.54	6.22	

From the table 4.5, the result of in vivo: comparison study is shown the result in the same way as phantom study. All T_2 are not significantly different between TR and sequences. (The results of T_2 comparison exceeding 10 percent difference are assumed to be significantly different [25].)

4.3.2 Exercise study data

The muscle MR images were generated using two pulse sequences, SE-EPI by optimized TR (TR = 1,000 ms) was used to calculate T_2 and TrueFISP image was used to obtain morphological information. The signal intensities were measured by determining ROIs in the area of tibialis anterior muscle [TA] and gastrocnemius muscle [GA] at rest and after exercise. T_2 were calculated using mono-exponential linear least-squares methods of TE = 30, 45, 60, 75 ms. T_2 of in vivo: exercise study are presented in table 4.6 and 4.7.

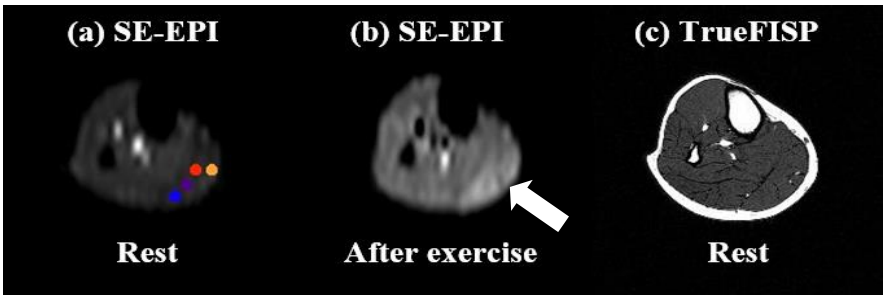

Figure 4.7 Representative MR images of the right lower leg of SE-EPI at rest (a) and after exercise (b) and TrueFISP image at rest (c). The arrows indicate the areas of activated muscle.

From figure 4.7a, the example of 4 ROIs are placed on the area of the gastrocnemius muscle [GA] at rest. The ROIs are mapped at the same region of the after exercise images as well. The changes in signal intensity after exercise shows the activation of gastrocnemius muscle [GA] in figure 4.7b (arrow). TrueFISP image display the morphological information well in figure 4.7c.

Table 4.6 T_2 of in vivo: exercise study from 8 healthy male volunteers at rest and after exercise of tibialis anterior muscle [TA] and gastrocnemius muscle [GA].

Subject No.	T_2 (ms)			
	Rest		After exercise	
	TA	GA	TA	GA
1	31.98	35.04	32.03	38.25
2	30.99	32.58	30.97	36.12
3	32.98	31.16	32.60	35.12
4	31.74	28.78	37.91	39.71
5	27.98	30.16	35.31	39.84
6	30.39	30.70	31.74	32.86
7	31.23	32.32	31.27	37.66
8	29.72	30.17	30.12	37.48
Mean±SD	30.88±1.54	31.36±1.93	32.74±2.59	37.13±2.36

Table 4.7 The muscle T_2 at rest and after exercise of tibialis anterior muscle [TA] and gastrocnemius muscle [GA].

	T_2 (ms)	
Muscle	Rest	After exercise
TA	30.88 ± 1.54	32.74 ± 2.59
GA	31.36 ± 1.93	37.13 ± 2.36

From table 4.7, the paired t-test was used to determine the statistical difference between T_2 at rest and after exercise; $P<0.05$ was considered significant. For gastrocnemius muscle [GA], T_2 after exercise is significantly higher than T_2 at rest ($P = 0.001$). There is no significantly different between rest and after exercise in Tibialis anterior muscle [TA] ($P = 0.129$). The changes in T_2 drastically increases in GA muscle and slightly increases in Tibialis anterior muscle [TA].

CHAPTER 5

DISCUSSION AND CONCLUSIONS

5.1 Discussion

The mfMRI is noninvasive technique that used to measure the changes in T_2 of muscle tissue after specific exercise. Different sequences can be used, MSE sequences are mostly applied to calculate T_2. However, the sequence usually require several minute to acquire image data. Though SE-EPI is an innovative technique to reduce the acquisition time for calculating T_2, there are few reports about the extensive comparative evaluation of the imaging parameters of SE-EPI sequence. Therefore, the optimization of image conditions for calculating T_2 still remains controversial.

The main purpose of this study was to study the effect of TR during the muscle T_2 measurement to decrease scan time when comparing MSE to SE-EPI sequences at 1.5 Tesla MRI. The result in each TRs were compared by T_2 relaxation curve and T_2.

5.1.1 Phantom study

For MSE, MR signal of MSE increased with increasing TR. The signal intensity curve of TR = 1,000 ms is lower than the other TR's signals. The reason is that the effect of low SNR in a short TR because of incomplete recovery of longitudinal magnetization. Although, the relaxation curve of TR = 1,000 ms demonstrating MR signal was lower than the other TR, all value is no significant difference between TR and sequences when all T_2 was compared. In this study, the results of T_2 comparison exceeding 10 percent of the T_2 were assumed to be significant [25].

For SE-EPI, T_2 relaxation curve of all TR is almost as same. Since SE-EPI used for this experiment is single-shot SE-EPI, every data collection is completed with one TR. When T_2 relaxation curve of MSE and SE-EPI were compared the MR signals of SE-EPI is less than MSE. The reason is that SE-EPI involves a pulse sequence in which fat saturation is applied until the pre-RF pulse. Therefore, the fat MR signal was suppressed on SE-EPI images.

5.1.2 In vivo: comparison study

For in vivo: comparison study, the effect of TR on calculating T_2 had shown result in the same way as the phantom study. When T_2 relaxation curve of MSE and SE-EPI were compared MR signals of TE longer than 90 ms, it was found that MR signals were not at the same gradients between MSE and SE-EPI. Due to skeletal muscle of human is not a single material, and is short T_2. It is supposed that MR signal of SE-EPI was influenced by not only T_2 relaxation but also T_2-star (T_2*) relaxation, and these results agreed with the previous studies [20]. In addition, MR signal more than 180 ms in SE-EPI was nearly a plateau, was not an exponential curve. The reason is that this part of the plateau in SE-EPI is approximately the content of noise, and supports the previous report [20]. The effect of noise is not occured in PVA-gel relaxation curve because PVA-gel's T_2 is longer than muscle T_2. In other words, the case of signal intensity of PVA-gel has high SNR than the muscle. The level of MR signal of PVA-gel is higher than the signal level of noise, so the noise signal is not occur in PVA-gel relaxation curve.

The application of improvement of reducing the scanning time that focused on TR in MSE has been extensively reported in the literature [23, 28]. However, the question of the influence to calculated T_2 by short TR remains unsettled.

Furthermore, Tawara and colleagues [20, 21] investigated the feasibility of calculating T_2 from SE-EPI compare with MSE. The study does not examine the imaging conditions for calculating T_2 (especially TR), even though precision of T_2 calculated by mono-exponential linear least-squares regression is influenced by the signal-to-noise ratio (SNR). They only use TR = 2,000 ms. Our data shows that TR = 1,000 ms on the MSE and SE-EPI can be used on muscle T_2 measurement without the difference in T_2.

5.1.3 In vivo: exercise study

The second purpose was to investigate the feasibility of shortening scan time technique of T_2 measurement to detect the muscle activity that induced by exercise.

Almost previous studies about exercise induced muscle activity used SE or MSE to calculate T_2 [29-31]. They had limitation about scanning time, about 4 minutes per series or more, which can be possible to examine only in extremity muscle.

Figure 4.7 shows transverse MR images of the right lower leg at rest and after exercise. Figure 4.7b illustrate increasing of water contain in gastrocnemius muscle [GA], Ankle plantar flexion induced the activation in GA than T_2 at rest and other muscle around it [21, 32-34]. Regarding the difference by exercise between rest and after exercise was not measured by T_2, and the results of this study differ from the previous studies [21], the exercise protocol had not made the strict settings when compared to the other's reports. Therefore, the cause was suggested that it was possible to have been under load in addition to the target muscle. It is the limit of this study.

Finally, we recommend that the SE-EPI can be used to investigate the muscle activity that induced by exercise.

5.2 Conclusions

MR images presented with a short TR (TR=1,000 ms) under suitable condition are possible to calculate muscle T_2 on mfMRI to reduce the scanning time dramatically. Calculating T_2 using SE-EPI sequence can be applied to detect the muscle activity that induced by exercise with the shortening acquisition time technique of approximately 1/17 of the previous method and can be acquired on the muscles of the trunk in a single breath-hold.

REFERENCES

1. Cagnie, B., et al., Muscle functional MRI as an imaging tool to evaluate muscle activity. J Orthop Sports Phys Ther, 2011. 41(11): p. 896-903.
2. Crema, M.D., F.W. Roemer, and A. Guermazi, Advanced MRI of Muscles in Sports Medicine. Aspetar Sports Medicine Journal, 2015. 4: p. 348-352.
3. Crema, M.D., et al., Imaging techniques for muscle injury in sports medicine and clinical relevance. Curr Rev Musculoskelet Med, 2015. 8(2): p. 154-61.
4. Meyer, R.A. and B.M. Prior, Functional magnetic resonance imaging of muscle. Exerc Sport Sci Rev, 2000. 28(2): p. 89-92.
5. Brown, M.A. and R.C. Semelka, eds. MRI : basic principles and applications 3rd ed. 2003, John Wiley & Sons, Inc.: Canada.
6. Tsao, C. Basic MRI Physics. 2008; Available from: http://wikidoc.org/index.php/Basic_MRI_Physics.
7. McRobbie, D.W., et al., MRI From Picture to Proton. 2007, Cambridge University Press: New York, United States of America
8. Lindberg, J. and M. Horn, MRI relaxation measurements in rats and mice, in Department of radiation physics. 2008, University of Gothenburg: University of Gothenburg.
9. Berry, E. and J.A. Bulpitt, Fundamentals of MRI: An Interactive Learning Approach. Medical Physics and Biomedical Engineering, ed. J.G. Webster, et al. 2008: CRC Press, Taylor & Francis Group.
10. Gould, T.A. and M. Edmonds. How MRI Works: MRI Magnets: the Major Players. 2008; Available from: http://science.howstuffworks.com/mri1.htm.
11. Blink, J.E. Basic MRI : Physics. 2004; Available from: http://www.mri-physics.net.
12. Damon, B.M. and J.C. Gore, Physiological basis of muscle functional MRI: predictions using a computer model. J Appl Physiol (1985), 2005. 98(1): p. 264-73.

13. Donahue, K.M., et al., Simultaneous gradient-echo/spin-echo EPI of graded ischemia in human skeletal muscle. J Magn Reson Imaging, 1998. 8(5): p. 1106-13.
14. Fleckenstein, J.L., et al., Absence of exercise-induced MRI enhancement of skeletal muscle in McArdle's disease. J Appl Physiol (1985), 1991. 71(3): p. 961-9.
15. Fisher, M.J., et al., Direct relationship between proton T2 and exercise intensity in skeletal muscle MR images. Invest Radiol, 1990. 25(5): p. 480-5.
16. Yue, G., et al., Sensitivity of muscle proton spin-spin relaxation time as an index of muscle activation. J Appl Physiol (1985), 1994. 77(1): p. 84-92.
17. Conley, M.S., et al., Noninvasive analysis of human neck muscle function. Spine (Phila Pa 1976), 1995. 20(23): p. 2505-12.
18. Fleckenstein, J.L., et al., Acute effects of exercise on MR imaging of skeletal muscle in normal volunteers. AJR Am J Roentgenol, 1988. 151(2): p. 231-7.
19. Akima, H., et al., Coactivation pattern in human quadriceps during isokinetic knee-extension by muscle functional MRI. Eur J Appl Physiol, 2004. 91(1): p. 7-14.
20. Tawara, N., O. Nitta, and A. Itoh, Comparison of pulse sequences for T_2 measurement of human skeletal muscle. Jpn J Magn Reson 2008. 28: p. 25-34.
21. Tawara, N., et al., T_2 mapping of muscle activity using ultrafast imaging. Magn Reson Med Sci, 2011. 10(2): p. 85-91.
22. Hedeker, D., R.D. Gibbons, and C. Waternaux, Sample Size Estimation for Longitudinal Designs with Attrition: Comparing Time-Related Contrasts Between Two Groups. Journal of Educational and Behavioral Statistics, 1999. 24: p. 70-93.
23. Tawara, N., et al., Complications related to repetition time during the measurement of muscle T_2 in 3.0 Tesla. In Proceedings of the 18th Annual Scientific Meeting of Korea Society for Magnetic Resonance in Medicine, 2013. 18: p. 207.
24. Price, R., et al., Magnetic Resonance Imaging QUALITY CONTROL MANUAL. 2015, American College of Radiology.

25. Kjaer, L., et al., Evaluation of relaxation time measurements by magnetic resonance imaging. A phantom study. Acta Radiol, 1987. 28(3): p. 345-51.
26. Schneiders, N.J., et al., Accurate T2 NMR images. Med Phys, 1983. 10(5): p. 642-5.
27. Johnson, G., et al., Accuracy and precision in the measurement of relaxation times from nuclear magnetic resonance images. Br J Radiol, 1987. 60(710): p. 143-53.
28. Laule, C., et al., In vivo multiecho T2 relaxation measurements using variable TR to decrease scan time. Magn Reson Imaging, 2007. 25(6): p. 834-9.
29. Akima, H., R. Kinugasa, and S. Kuno, Recruitment of the thigh muscles during sprint cycling by muscle functional magnetic resonance imaging. Int J Sports Med, 2005. 26(4): p. 245-52.
30. Cagnie, B., et al., Functional reorganization of cervical flexor activity because of induced muscle pain evaluated by muscle functional magnetic resonance imaging. Man Ther 2011. 16(5): p. 470-475.
31. Pearson, W.G., Jr., et al., Evaluating swallowing muscles essential for hyolaryngeal elevation by using muscle functional magnetic resonance imaging. Int J Radiat Oncol Biol Phys, 2013. 85(3): p. 735-40.
32. Disler, D.G., et al., Dynamic evaluation of exercising leg muscle in healthy subjects with echo planar MR imaging: work rate and total work determine rate of T2 change. J Magn Reson Imaging, 1995. 5(5): p. 588-93.
33. Jenner, G., et al., Changes in magnetic resonance images of muscle depend on exercise intensity and duration, not work. J Appl Physiol (1985), 1994. 76(5): p. 2119-24.
34. Kennan, R.P., T.B. Price, and J.C. Gore, Dynamic echo planar imaging of exercised muscle. Magn Reson Imaging, 1995. 13(7): p. 935-41.

APPENDICES

Appendix A: Case record form

Table A.1 Means signal intensities (Mean ± SD) in each TE of phantom study.

Study : Phantom study				
Sequence :				
TE (ms)	Means signal intensities (Mean ± SD)			
	TR 1,000 (ms)	TR 2,000 (ms)	TR 3,000 (ms)	TR 4,000 (ms)
15				
30				
45				
60				
75				
90				
105				
120				
135				
150				
165				
180				
195				
210				
225				
240				
255				
270				
285				
300				
315				
330				
345				
360				
375				
390				

Table A.2 T_2 of phantom study using MSE and SE-EPI by variation of TR.

Phantom study	ROIs	T_2 (ms)			
		TR 1,000 (ms)	TR 2,000 (ms)	TR 3,000 (ms)	TR 4,000 (ms)
MSE	1				
	2				
	3				
	4				
	Means±SD				
SE-EPI	1				
	2				
	3				
	4				
	Means±SD				

Table A.3 T_2 of phantom study using MSE and SE-EPI versus the percent difference in each TR and sequences.

Sequences	T_2 (ms)				% Difference
	TR 1,000 (ms)	TR 2,000 (ms)	TR 3,000 (ms)	TR 4,000 (ms)	
MSE (ms)					
SE-EPI (ms)					
% Difference					

Table A.4 Subject data of in vivo study.

Subject No.	Date of Birth	Age			Weight (cm.)	Height (kg.)
		Year	Month	Day		
1						
2						
3						
4						
5						
6						
7						
8						

Table A.5 Means signal intensities in each TE of in vivo: comparison study.

Study : In vivo: comparison study				
Subject No. :				
Sequence :				
TE (ms)	Means signal intensities (Mean ± SD)			
	TR 1,000 (ms)	TR 2,000 (ms)	TR 3,000 (ms)	TR 4,000 (ms)
15				
30				
45				
60				
75				
90				
105				
120				
135				
150				
165				
180				
195				
210				
225				
240				
255				
270				
285				
300				
315				
330				
345				
360				
375				
390				

Table A.6 T_2 of in vivo: comparison study using MSE and SE-EPI by variation of TR.

Sequences	Subject No.	T_2 (ms)			
		TR 1,000 (ms)	TR 2,000 (ms)	TR 3,000 (ms)	TR 4,000 (ms)
MSE	1				
	2				
	3				
	4				
	5				
	6				
	7				
	8				
	Means±SD				
SE-EPI	1				
	2				
	3				
	4				
	5				
	6				
	7				
	8				
	Means±SD				

Table A.7 T_2 of in vivo: comparison study using MSE and SE-EPI versus the percent difference values in each TR and sequences.

Sequences	T_2 (ms)				% Difference
	TR 1,000 (ms)	TR 2,000 (ms)	TR 3,000 (ms)	TR 4,000 (ms)	
MSE (ms)					
SE-EPI (ms)					
% Difference					

Table A.8 T_2 of in vivo: exercise study at rest and after exercise of tibialis anterior muscle [TA] and gastrocnemius muscle [GA].

Subject No.	T_2 (ms)			
	Rest		After exercise	
	TA	GA	TA	GA
1				
2				
3				
4				
5				
6				
7				
8				
Mean±SD				

Table A.9 T_2 at rest and after exercise of tibialis anterior muscle [TA] and gastrocnemius muscle [GA].

	T_2 (ms)	
Muscle	Rest	After exercise
TA		
GA		

Appendix B: Quality control of MRI scanner

Site location: 14 Floor building, King Chulalongkorn Memorial Hospital

Date: 20/05/2016

Equipment:

MRI System Manufacturer: Siemens

Model: MAGNETOM, Aera 1.5 Tesla

QC Phantom: ACR Phantom

Serial number: J11710

Quality of MRI system consists of seven contents

- Geometric accuracy
- High contrast spatial resolution
- Slice thickness accuracy
- Slice position accuracy
- Image intensity uniformity
- Percent signal ghosting
- Low contrast object detectability

Procedures the QC Phantom

Place the QC phantom on the head coil and level it. Turn “NOSE” side to tilt the top of phantom and turn “CHIN” side away from the gantry. Use the laser alignment lights to position the phantom.

The MRI accreditation program requires the acquisition of a sagittal localizer and four axial series of images. The same set of eleven slice locations within the phantom is required using the scanner’s head coil. The scan parameters for the localizer and the first two axial series of imaged are fully prescribed by ACR in the scanning instructions as the ACR sequence or ACR images. The third and fourth series of axial images based on King Chulalongkorn Memorial hospital is the spin echo T1 and

T2 protocols and are referred to set the sequences or site images. To discuss the image data it is convenient to introduce name for the different sets of image and numbering for the slice locations within the phantom.

The localizer is a 20 mm thick single slice spin echo acquisition through the center of phantom, and is referred to simply as the **localizer**.

The first axial series is a spin echo acquisition with ACR specified scan parameters that are typical of T1-weighted acquisitions. This series is called the **ACR T1** series.

The second axial series is a double spin echo acquisitions with ACR specified scan parameters that are typical of proton density/T2-weighted acquisitions. When analyzing data from this acquisition only the second-echo image are used. The set of second-echo image from this acquisition is called the **ACR T2** series.

The third and fourth axial series are based on the scan parameters at King Chulalongkorn Memorial Hospital normally used its clinical protocols for axial head T1 and head T2 weighting. These series are called the **clinical T1** and **clinical T2**.

Table B.1 ACR pulse sequence acquisition parameters.

Study	Pulse sequences	TR (ms)	TE (ms)	FOV (cm)	No. of slices	Thickness (mm)	Slice gap (mm)	NSA	Matrix	Bandwidth (kHz)	Scan time (min:sec)
Sagittal locator	Spin Echo	200	20	25	1	20	N/A	1	256x256	285	0:53
ACR Axial T1	Spin Echo	500	20	25	11	5	5	1	256x256	115	2:07
ACR Axial T2	Spin Echo	2000	20 80	25	11	5	5	1	256x256	115	8:29
Clinical Axial T1	Spin Echo	500	8.9	24	28	5	0	1	288x384	150	2:23
Clinical Axial T2	Turbo Spin Echo	6070	74	24	28	5	0	1	336x448	200	1.31

B.1. Geometric accuracy

Purpose: To assess the accuracy of the image represents lengths in the imaged subject.

Method:

1. Display the localizer, measure the end-to-end length of the phantom as it appears in the localizer (line No.1).
2. Display slice 1 of the ACR T1 series. Measure the diameter of the phantom in 2 directions: top-to-bottom (line No.2) and left-to-right (line No.3).
3. Display slice 5 of the ACR T1 series. Measure the diameter of the phantom in 4 directions: top-to-bottom (line No.4), left-to-right (line No.5), and both diagonals (line).

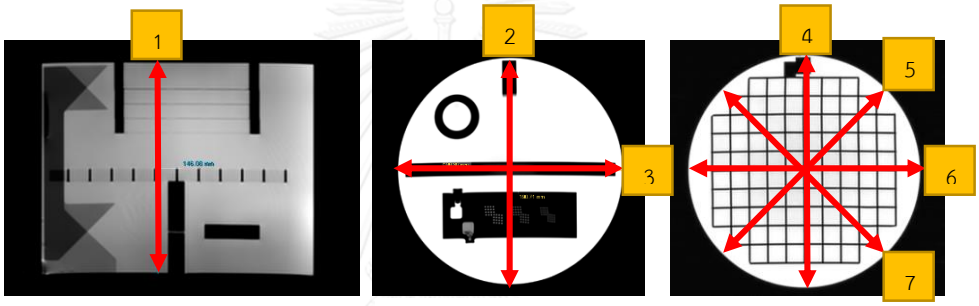

Sagittal locator Slice 1 Slice 5

Figure B.1 The end-to-end length and diameter measurements illustrated.

Table B.2 Geometric accuracy test result.

Line No.	True value (mm)	Sagittal Locator		ACR T1		ACR T2		Clinical T1		Clinical T2	
		Meas. (mm)	Diff. (mm)	Meas. (mm)	Diff. (mm)	Meas. (mm)	Diff. (mm)	Meas. (mm)	Diff. (mm)	Meas. (mm)	Diff. (mm)
1	148	147.75	-0.25								
2	190			191.35	+1.35	191.35	+1.35	191.05	+1.05	191.05	+1.05
3	190			189.25	-0.75	189.25	-0.75	189.85	-0.15	189.45	-0.55
4	190			191.35	+1.35	191.7	+1.7	191.84	+1.84	191.44	+1.44
5	190			190.72	+0.72	190.97	+0.97	190.54	+0.54	190.25	+0.25
6	190			189.25	-0.75	190.65	+0.65	189.85	-0.15	189.05	-0.95
7	190			190.47	+0.47	191.7	+1.7	190.82	+0.82	190.54	+0.54

Recommended criteria: All measured dimension should be within ±2 mm of their true values.

Result: PASSED

B.2. High contrast spatial resolution

Purpose: To assess the scanner's ability to resolve small objects when the contrast-to-noise ratio is sufficiently high.

Method: For this test, resolution in slice 1 of each of the 2 ACR axial series is evaluated. The following procedure is repeated for each of those series:

1. Display the slice 1 ACR axial series and magnify the image by a factor of between 2 and 4.
2. Look at the rows of hole in the UL (Upper Left) array, and adjust the display window and level to best show the holes as distinct from one another.
3. Score the image as resolved right to left at this particular hole size. Look at the holes in the LR (lower right) array and adjust the display window and level to best show the holes as distinct from one another.
4. Make a note of the smallest hole size resolved in each direction.

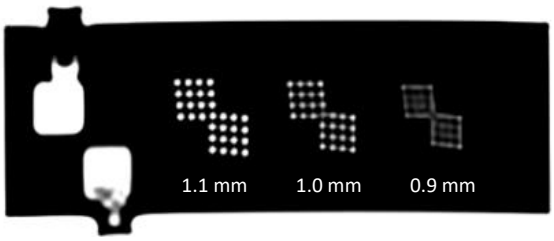

Figure B.2 Magnified portion of slice 1 displayed appropriately for visually assessing high contrast resolution.

Table B.3 High contrast spatial resolution result.

Sequence	Resolution	Result
ACR T1	1 mm	Pass
ACR T2	1 mm	Pass
Clinical T1	0.9 mm	Pass
Clinical T2	0.9 mm	Pass

Recommended action criteria: the measured resolution should be 1.0 mm or better.

Result: PASSED

B.3. Slice thickness accuracy

Purpose: To assess the accuracy of a slice of specified thickness. The prescribed slice thickness is compared with the measured slice thickness.

Method: For slice thickness accuracy the lengths of 2 signal ramps in slice 1 are measured. The ramps appear in a structure called the slice thickness insert. The 2 ramps are crossed: one has a negative slope and the other a positive slope with respect to the plane of slice 1. They are produced by cutting 1 mm wide slots in a block of plastic. The slots are open to the interior of the phantom and are filled with the same solution that fills the bulk of the phantom. The signal ramps have a slope of 10 to 1 with respect to the plane of slice 1 that is they make an angle of about 5.71° with slice 1. Therefore, the signal ramps will appear in the image of slice 1 with a length that is 10 times the thickness of the slice. If the phantom is tilted in the right-left direction, one ramp will appear longer than the other. Having crossed ramps allows for correction of the error introduced by right-left tilt.

For each ACR series, the length of the signal ramps in slice 1 is measured according to the following procedure:

1. Display slice 1, and magnify the image by a factor of 2 to 4. Adjust the display level so that the signal ramps are well visualized. The ramp signal is much lower than surrounding water.

2. Place a rectangular ROI at the middle of each signal ramp as shown in Figure 3. Note the mean signal values for each of these 2 ROIs then average those 2 values together. The result is a number approximating the mean signal in the middle of the ramps.

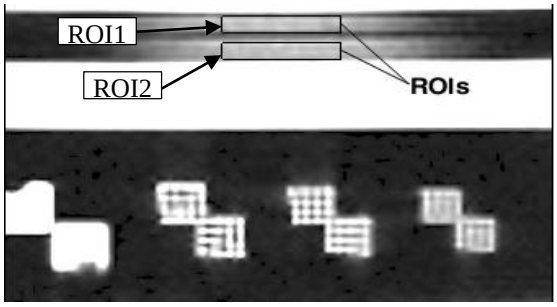

Figure B.3 ROIs placed for measuring average signal in the ramps.

3. Display level to half of the average ramp signal calculated. Use the on-screen length measurement tool of the display station to measure the lengths of the top and bottom ramps. Record these lengths.

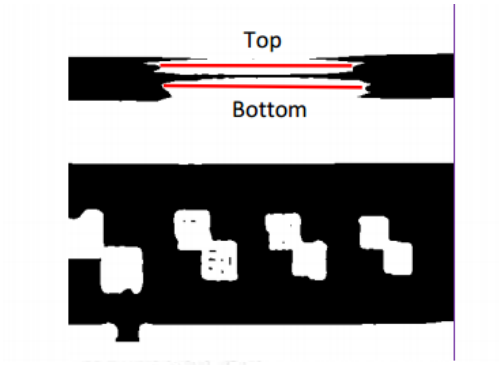

Figure B.4 Magnified region of slice 1 showing slice thickness signal ramps.

4. The slice thickness is calculated using the following formula

$$Slice\ thickness = 0.2 \times \frac{(top \times bottom)}{(top + bottom)} \quad \text{(B.1)}$$

Table B.4 Slice thickness accuracy test result.

Sequence	Slice Thickness Setting (mm)	Slice Thickness Measurement (mm)	Difference (mm)	Result
ACR T1	5	5.04	+ 0.04	Pass
ACR T2	5	5.25	+ 0.25	Pass
Clinical T1	5	5.07	+ 0.07	Pass
Clinical T2	5	5.59	+ 0.59	Pass

Recommended action criteria: The measured thickness should be 5.0 ±0.7mm

Result: PASSED

B.4. Slice position accuracy

Purpose: To assesses the accuracy with which slices can be prescribed at specific locations utilizing the localizer image for positional reference.

Method: Slice position accuracy test the differences between the prescribed and actual positions of slices 1 and 11 are measured. These measurements are made for the ACR T1 and T2 series. The slices 1 and 11 are prescribed so as to be aligned with the vertices of the crossed 45° wedges at the inferior and superior ends of the phantom respectively. On slices 1 and 11 the crossed wedges appear as a pair of adjacent, dark, vertical bars at the top (anterior side) of the phantom. For both slice 1 and slice 11, if the slice is exactly aligned with the vertex of the crossed wedges, then the wedges will appear as dark bars of equal length on the image. By design of the wedges, if the slice is displaced superiorly with respect to the vertex, the bar on the observer's right (anatomical left) will be longer. If the slice is displaced inferiorly with respect to the vertex, the bar on the left will be longer.

Measurements are made for slices 1 and 11 of the ACR T1 and ACR T2 series. Use the following procedure for each image:

1. Display the slice. Magnify the image by a factor of 2 to 4, keeping the vertical bars of the crossed wedges within the displayed portion of the magnified image.

2. Adjust the display window so the ends of the vertical bars are well defined and use the on-screen length measurement tool to measure the difference in length between the left and right bars. The length to measure is indicated by the arrows in Figure B.6.

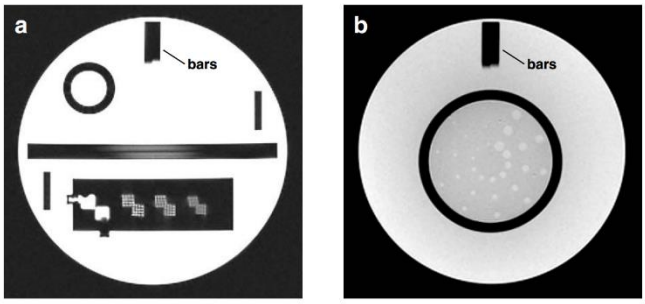

Figure B.5 Images of slice 1 (a) and slice 11 (b) with the pairs of vertical bars from the 45° crossed wedges indicated.

On these images the length difference between the right and left bars is small and typical of well-positioned slices.

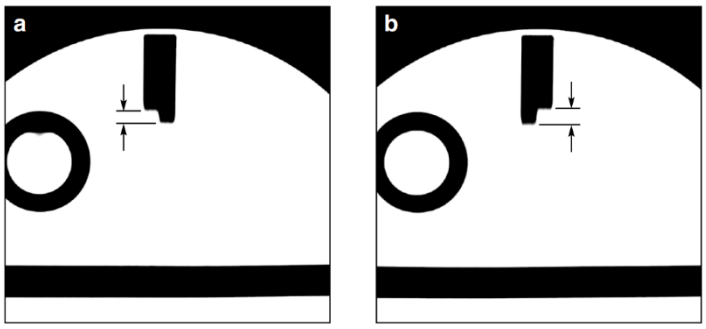

Figure B.6 Images of slice 1 illustrating measurement of slice position error. The arrows indicate the bar length difference measurement that is to be made.

(a) The bar on the right is longer, meaning the slice is mispositioned superiorly; this bar length difference is assigned a positive value (+).

(b) The bar on the left is longer, meaning the slice is mispositioned inferiorly; this bar length difference is assigned a negative value (-).

Table B.5 Slice position accuracy test result.

Sequence	Slice 1	Slice 11	Result
ACR T1	1.40	-2.92	Pass
ACR T2	0.53	-2.56	Pass
Clinical T1	0.98	-2.52	Pass
Clinical T2	0.89	-2.53	Pass

Recommended action criteria: The magnitude of each bar length difference should be less or equal to 5 mm.

Result: PASSED

B.5. Image intensity uniformity

Purpose: To measures the uniformity of the image intensity over a large water-only region of the phantom lying near the middle of the imaged volume and thus near the middle of the head coil

Method:

1. Display slice location 7.
2. Place a large, circular region-of-interest (ROI) on image. This ROI should have an area of between 195 cm^2 and 205 cm^2.
3. Set the display window to its minimum, and lower the level until the entire area inside the large ROI is white.
4. Place the small ROI roughly 1 cm^2 at the region of dark pixels develops inside the large ROI.
5. Record the mean pixel value for this 1 cm^2 ROI. This is the measured low-signal value.
6. Raise the level until all but a small, roughly 1 cm^2 region of white pixels remains inside the large ROI. This is the region of highest signal.
7. Record the average pixel value for this 1 cm^2 ROI. This is the measured high-signal value.

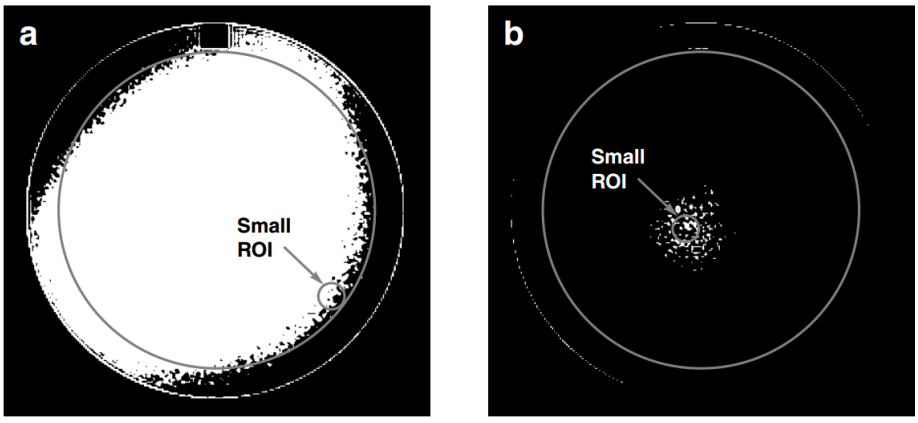

Figure B.7 (right) ROI placement for low signal-value, (left) ROI placement for High signal-value.

The measured high-and low-signal values for each of the ACR series are combined to produce a value called percent integral uniformity (PIU). Use the following formula to calculate PIU:

$$PIU = 100 \times \left(1 - \frac{(high - low)}{(high + low)}\right) \quad \text{(B.2)}$$

Table B.6 Image intensity uniformity test result.

Sequence	Low signal	High signal	PIU (%)	Result
ACR T1	1578	1751	94.8	Pass
ACR T2	1182	1320	94.4	Pass
Clinical T1	1219	1353	94.7	Pass
Clinical T2	1016	1113	95.4	Pass

Recommended action criteria: PIU should be greater than or equal to 87.5% for MRI systems with field strengths less than 3 Tesla.

Result: PASSED

B.6. Percent signal ghosting

Purpose: To assesses the level of ghosting in the image.

Method:

1. Percent signal ghosting measurements are made on slice 7 of the ACR T1 series.
2. Using the workstation's ROI tool, 5 intensity measurements are made: the average intensity in the primary image of the phantom, and the average intensity in the background at 4 locations outside of the phantom.
3. The value for the ghosting, as a fraction of the primary signal, is calculated using the following formula:

$$Ghosting\ ratio = \frac{(top+btm)-(left+right)}{(2\times Large\ ROI)} \quad \text{(B.3)}$$

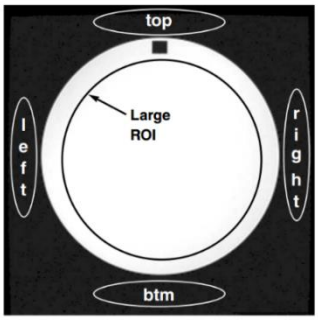

Figure B.8 ROIs placement for percent-signal ghosting measurements.

Table B.7 Pixel value and Percent signal ghosting test result.

Sequence	Top	Bottom	Left	Right	Large	Calculated value	Result
ACR T1	8.25	9.64	8.48	9.04	1669	0.00011	Pass
ACR T2	8.34	8.08	9.18	11.55	1264	0.0017	Pass
Clinical T1	7.03	8.16	6.45	5.8	1310.37	0.0011	Pass
Clinical T2	9.11	9.93	11.3	9.03	1076.63	0.00059	Pass

Recommended action criteria: The ghosting ratio should be less than or equal to 0.025.

Result: PASSED

B.7. Low contrast object detectability

Purpose: To assesses the extent to which objects of low contrast are discernible in the images.

Method: The low-contrast objects appear on 4 slices: slices 8 through 11. In each slice the low-contrast objects appear as rows of small disks, with the rows radiating from the center of a circle like spokes in a wheel. Each spoke is made up of three disks, and there are ten spokes in each circle. All the disks on a given slice have the same level of contrast. In order, from slice 8 to slice 11, the contrast values are 1.4%, 2.5%, 3.6%, and 5.1%. All the disks in a given spoke have the same diameter. Starting at the 12 o'clock position and moving clockwise, the disk diameter decreases progressively from 7.0 mm at the first spoke to 1.5 mm at the tenth spoke.

The measurements for this test consist of counting the number of complete spokes seen in each of the four slices. This is done for each of the four axial series. Use the following procedure to score the number of complete spokes seen in a slice:

1. Display the slice to be scored. It helps to start with slice 11, which has the highest contrast objects.
2. Adjust the display window width and level settings for best visibility of the low-contrast objects.
3. Count the number of complete spokes. Begin counting with the spoke having the largest diameter disks. Count clockwise from spoke 1 until a spoke is reached where 1 or more of the disks is not discernible from the background.

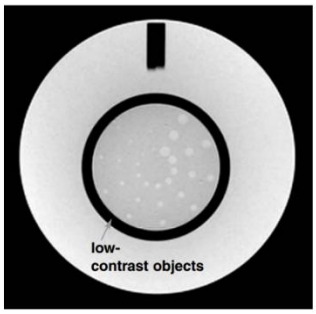

Figure B.9 Image of slice 11 showing the circle of low contrast objects for the low-contrast object detectability test.

Table B.8 Low contrast detectability test result.

Sequence	Contrast Value					Result
	1.40%	2.50%	3.60%	5.10%	Total	
ACR T1	7	10	10	10	37	Pass
ACR T2	6	8	9	10	33	Pass
Clinical T1	7	10	10	10	37	Pass
Clinical T2	2	8	9	10	29	Pass

Recommended action criteria: For both in the ACR series and clinical series should have a total score of at least 9 spokes for MRI systems with field strengths less than 3 Tesla.

Result: **PASSED**

Appendix C: T_2 calculation method

In this study, mono-exponential linear least-squares methods was performed to calculate T_2. The measured values are assumed to approximately correspond to the linear functional dependence. T_2 relaxation curve equation of the material that has single T_2 relaxation time is as follows.

$$y = M_0 \times e^{-(\frac{TE}{T_2})} \quad \text{(C.1)}$$

where M_o is signal intensity from MR images in TE = 0 ms, TE is time of echo (ms), T_2 is T_2 relaxation time (ms)

The following is the formula is deformed by the function of the natural logarithms.

$$\ln y = \ln M_0 - (\frac{TE}{T_2}) \quad \text{(C.2)}$$

$$\ln y = \ln M_0 - (\frac{1}{T_2}) \times TE \quad \text{(C.3)}$$

Here, ln y = Y, ln M_o = B, and $1/T_2$ = A is assigned to the above function and it becomes the linear function equation.

$$\mathrm{Y} = -A \times TE + B \quad \text{(C.4)}$$

Thus, T_2 is obtained in the form

$$T_2 = \frac{1}{A} \quad \text{(C.5)}$$

VITA

NAME	Mr. Patompong Polharn
NATIONALITY	Thai
DATE OF BIRTH	6 April 1987
PLACE OF BIRTH	Amnatcharoen, Thailand
EDUCATION	Bachelor of Science in Radiological Technology, Faculty of Medical Technology, Mahidol University, 2010
WORK EXPERIENCES	2010-Present Radiological Technologist, Somdech Phra Debaratana Medical Center, Faculty of Medicine, Ramathibodi Hospital
ADDRESS	695/552 Prachachuen Road., Bang Sue, Bangkok, Thailand 10800
E-mail	oofzid3@gmail.com